

NUMERICAL BIFURCATION STUDY OF SUPERCONDUCTING PATTERNS ON A SQUARE

NICO SCHLÖMER*, DANIELE AVITABILE[†], AND WIM VANROOSE[‡]

Abstract. This paper considers the extreme type-II Ginzburg–Landau equations that model vortex patterns in superconductors. The nonlinear PDEs are solved using Newton’s method, and properties of the Jacobian operator are highlighted. Specifically, it is illustrated how the operator can be regularized using an appropriate phase condition. For a two-dimensional square sample, the numerical results are based on a finite-difference discretization with link variables that preserves the gauge invariance. For two exemplary sample sizes, a thorough bifurcation analysis is performed using the strength of the applied magnetic field as a bifurcation parameter and focusing on the symmetries of this system. The analysis gives new insight in the transitions between stable and unstable states, as well as the connections between stable solution branches.

Key words. Superconductors, Ginzburg–Landau system, symmetry-breaking bifurcations, vortices, regularization.

1. Introduction. In this article, we study the symmetry-breaking transitions between stable and unstable patterns in small-sized superconducting samples. Superconductors are materials that expel magnetic fields and exhibit zero electrical resistance when they are below a characteristic temperature T_c . Mathematically, the superconductor’s states are described by a set of nonlinear PDEs, known as the Ginzburg–Landau system [21].

For simplicity, let us suppose that a sample of superconducting material occupies an open, bounded region Ω of the Euclidean space, immersed in an external magnetic field \mathbf{H}_0 (see Figure 1.1). Above a critical temperature T_c , the material behaves like a normal conductor: it exhibits electrical resistivity and is homogeneously penetrated by the applied magnetic field. The material is said to be in a *homogeneously non-superconducting state* (or *normal state*).

At low temperatures, $T < T_c$, the material exhibits a *complete* loss of resistivity, resulting in the formation of superconducting currents in the sample. Such currents give rise to an induced magnetic field and the total magnetic field \mathbf{B} is expelled from the interior of the sample. Below a certain critical field strength H_{c1} , the magnetic field is expelled entirely; the material is said to be in a *homogeneously superconducting state*. Below the critical temperature and for stronger applied magnetic fields, however, mixed configurations can exist: the magnetic field penetrates only in confined regions of the sample. For so-called *type-II superconductors* [25], those areas are circular *vortices*, arranged in characteristic patterns.

In large samples, the vortices organize in a regular pattern, also known as the *Abrikosov lattice* (see [1], [25] and references therein). In small samples, however, owing to the boundaries, the observed patterns can significantly deviate from the regular lattice and their organization depends sensitively on the intensity of the applied magnetic field as well as the geometry and the symmetries of the sample. These small-scale (mesoscopic) systems with simple geometric shapes like discs, triangles, or squares are of technological interest since they can be built into nanoscale devices [5].

*Departement Wiskunde-Informatica, Universiteit Antwerpen, Middelheimlaan 1, 2020 Antwerpen, Belgium

[†]Department of Mathematics, University of Surrey, Guildford, GU2 7XH, UK

[‡]Departement Wiskunde-Informatica, Universiteit Antwerpen, Middelheimlaan 1, 2020 Antwerpen, Belgium

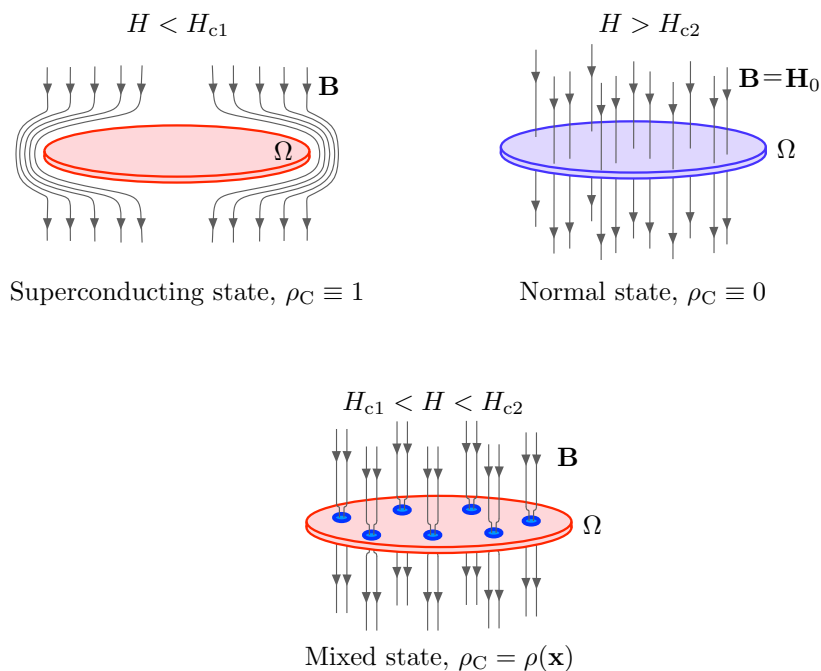


Fig. 1.1: States of a superconducting sample immersed in an external magnetic field \mathbf{H}_0 . Top: below the critical temperature and for $H < H_{c1}$, the sample is in a homogeneously superconducting state in which internal currents are generated and the total magnetic field \mathbf{B} is expelled from the specimen (left); above the critical temperature or for $H > H_{c2}$, the material is in a normal state and the external magnetic field penetrates the whole sample (right). Bottom: type-II superconductors can exhibit mixed states, in which vortices of normal conductivity are embedded in a superconductive background. In the mixed configuration, \mathbf{B} can penetrate the sample only through the vortices, giving rise to characteristic superconductive patterns.

In applications, one is interested in finding steady states of the system, studying their stability and their dependence upon the external magnetic field. The state of a superconducting sample is, in general, characterized by two quantities: the total magnetic field $\mathbf{B} =: \mathbb{R}^3 \rightarrow \mathbb{R}^3$ and the density $\rho_C: \Omega \cup \partial\Omega \rightarrow \mathbb{R}$ of electron pairs which constitute superconductivity (Cooper pairs).

A typical approach for studying superconducting states is to define a suitable Gibbs energy for the system and to derive a set of evolution equations for the order parameter $\psi: \Omega \cup \partial\Omega \rightarrow \mathbb{C}$, $|\psi|^2 = \rho_C$, and the magnetic vector potential $\mathbf{A}: \mathbb{R}^3 \rightarrow \mathbb{R}^3$, $\nabla \times \mathbf{A} = \mathbf{B}$. The resulting system is known as the *Ginzburg–Landau system* [21]. The associated initial-boundary-value problem has been studied both analytically and numerically. Various results on the existence and uniqueness of solutions, for example, can be found in [10, 34, 32] and references therein.

However, it is often necessary to resort to numerical simulation to study the complex interaction of vortices in samples of arbitrary shapes: a popular strategy is to time-step the Ginzburg–Landau system via Gauss–Seidel iterations until an equilibrium is reached; the external magnetic field is then varied quasi-statically, and a

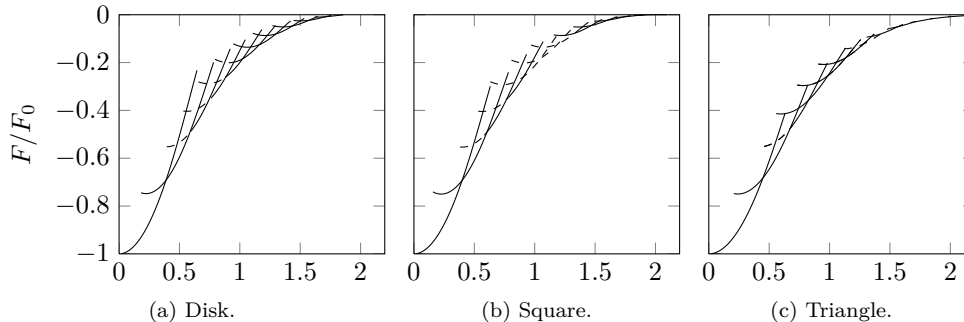


Fig. 1.2: (Reproduced from [9].) Typical cascades of branches of steady states of the Ginzburg–Landau problem for various two-dimensional sample shapes. The plots show the strength of the applied magnetic field (homogeneous and perpendicular to the sample) versus the normalized energy of the states.

new steady state is found [9, 35]. We show a typical result of this analysis in Figure 1.2. The solution branches appear disconnected: when an instability is met, the direct simulation jumps to a nearby stable branch, as the employed numerical method can compute only stable solutions.

The plots in Figure 1.2 are in good agreement with the hysteretic behavior that has also been observed experimentally [36], but they are not yet fully understood from the point of view of bifurcation analysis. The main results in this direction are confined to one-dimensional spatial domains (see [17, 4, 2] and references therein). The two-dimensional case has been studied by means of direct numerical simulation for various material parameters and strengths of the applied magnetic field [3], as well as for a variety of different shapes and domain sizes (see [19, 9, 13] and references therein), but the bifurcation scenario of the Ginzburg–Landau problem in two and three dimensions is largely unexplored.

The main motivation of the present paper is to classify the instabilities occurring in superconducting samples using numerical continuation, as opposed to time-dependent simulations. To this end, we define a well-posed boundary-value problem, choose a spatial discretization, and find steady states of the Ginzburg–Landau problem by Newton iterations. More specifically, we focus on square samples of extreme type-II superconductors subject to a homogeneous external magnetic field. In this case, the Ginzburg–Landau problem simplifies considerably as it is possible to derive the vector potential \mathbf{A} explicitly and then solve a nonlinear partial differential equation for the order parameter ψ .

We expect that the symmetries of the problem will influence the bifurcation landscape. As we will see, the relevant groups for the computations presented in this paper are the circle group S^1 and the dihedral group D_4 . The discrete D_4 symmetry suggests that we can use the *equivariant branching lemma* to predict symmetries of the emerging branches at bifurcation points [24, 27]. On the other hand, the continuous S^1 -symmetry induces the presence of a zero eigenvalue in the spectrum of the linear operator associated with the boundary-value formulation, causing problems to the convergence of the Newton iterations.

We regularize the system by extending the boundary-value problem and employing

a suitable phase condition, using the framework proposed by Champneys and Sandstede [14]. The extended boundary-value formulation is then discretized using a common gauge-preserving technique and the patterns are path-followed in parameter space via pseudo-arclength continuation.

To the best of our knowledge, this approach has never been employed before for the Ginzburg–Landau problem, albeit the application of Newton’s method has been proposed in [21] and inexact Newton methods are often used in practice [28]. In addition, equivariant bifurcation theory has never been used to explain the instabilities found experimentally and numerically in superconducting samples, even though the importance of symmetries was pointed out in [15], where the system is linearized around the trivial steady state and the relative eigenmodes are studied in the context of C_4 -symmetries.

The main result of the present paper is a classification of the bifurcations occurring in square domains of small and moderate sizes. In small samples, where the domain can host just a single superconducting vortex, the bifurcations are entirely determined by the natural two-dimensional irreducible representation of D_4 (see [27], Section 4.3). However, as the domain size increases, the bifurcation diagram gets more complicated and it involves also one-dimensional irreducible representations of D_4 . Furthermore, in larger samples we compute stable vortices of higher multiplicity: these structures were previously found by direct numerical simulation [9], but their formation was still an open problem; our analysis shows that vortices with different multiplicity are all linked in parameter space via symmetry-breaking bifurcations. Furthermore, we used Newton-Krylov methods to solve the system, exploiting the properties of the Jacobian operator in the Krylov iterations.

The remainder of the article is organized as follows. Section 2 discusses the Ginzburg–Landau system in the large- κ limit and details its symmetries. Section 3 contains material on the linearization of the Ginzburg–Landau system and its self-adjointness, which is of importance for the numerical solution of the linear system associated with each Newton iteration. Section 4 is concerned with the regularization of the equations. Details on the discretization of the system with link variables and properties thereof can be found in Section 5. The numerical computations are included in Section 6, where we show families of solutions as a function of the strength of the applied magnetic field. We relate the bifurcations to the symmetries of the solutions with the help of the equivariant branching lemma. The appendix contains an extension of Keller’s bordering lemma which is used in Sections 4 and 5.

Notations. Throughout this article we will use bold symbols (\mathbf{x}) for vector-valued quantities. For any $z \in \mathbb{C}$, $\Re(z)$ and $\Im(z)$ denote its real and imaginary parts, \bar{z} is used for complex conjugation. Similarly, for $\psi : \Omega \rightarrow \mathbb{C}$, $\bar{\psi} : \Omega \rightarrow \mathbb{C}$ is such that $\bar{\psi}(x) := \overline{\psi(x)}$ for all $x \in \Omega$. For function spaces, we use $C^k(\Omega)$ denote the vector space of all k times differentiable functions. We use $L^2_{\mathbb{K}}(\Omega)$ for the Hilbert-space in the field \mathbb{K} of square-integrable functions over Ω , equipped with the inner product $\langle \varphi, \psi \rangle = \int_{\Omega} \overline{\varphi} \psi \, d\Omega$ for all $\varphi, \psi \in L^2_{\mathbb{K}}(\Omega)$. The range of a linear operator L is denoted by $\mathcal{R}(L)$. For the symmetry groups under consideration, the symbol S^1 is used to denote the circle group $\{z \in \mathbb{C} : |z| = 1\}$ (which is group-isomorphic to $\text{SO}(2)$). For a given state ψ , Σ_{ψ} denotes the symmetry group under the action of which ψ is invariant.

2. The Ginzburg–Landau equation. For an open, bounded domain $\Omega \subset \mathbb{R}^3$, with a piecewise smooth boundary $\partial\Omega$, the Ginzburg–Landau problem is usually

derived by minimizing the Gibbs free energy functional

$$G(\psi, \mathbf{A}) - G_n = \xi \frac{|\alpha|^2}{\beta} \int_{\Omega} \left[-|\psi|^2 + \frac{1}{2}|\psi|^4 + |-\mathbf{i}\nabla\psi - \mathbf{A}\psi|^2 + \kappa^2(\nabla \times \mathbf{A})^2 - 2\kappa^2(\nabla \times \mathbf{A}) \cdot \mathbf{H}_0 \right] d\Omega, \quad (2.1)$$

where the state (ψ, \mathbf{A}) is in the natural energy space such that the integral is well-defined [21]. As we have seen in the introduction, the scalar ψ is commonly referred to as the *order parameter*, while \mathbf{A} is the magnetic vector potential corresponding to the total magnetic field. The physical observables associated with the state (ψ, \mathbf{A}) are the density $\rho_C = |\psi|^2$ of the superconducting charge carriers and the total magnetic field $\mathbf{B} = \nabla \times \mathbf{A}$. The constant G_n represents the energy associated with the entirely normal (non-superconducting) state.

The energy (2.1) is written in its dimensionless form and it depends upon the impinging magnetic field \mathbf{H}_0 and the material parameters $\alpha, \beta, \kappa, \xi \in \mathbb{R}$. The most relevant parameters are κ and ξ ; in particular, $\kappa = \lambda/\xi$ is the ratio of the penetration depth λ (the length scale at which the magnetic field penetrates the sample) to the coherence length ξ (the characteristic spatial scale of ψ). A superconductor is said to be of *type I* if $\kappa < 1/\sqrt{2}$, and of *type II* otherwise.

To complete our description of the Gibbs energy, we remark that we have scaled the domain Ω in units of the coherence length ξ while another common choice is to scale the domain by λ [21].

Starting from the Gibbs energy and using standard calculus of variations, it is possible to derive the Ginzburg–Landau equations [21], a boundary-value problem in the unknowns ψ and \mathbf{A} . As anticipated in the introduction, we will simplify the problem and consider only the limit $\kappa \rightarrow \infty$ (*extreme type-II superconductors*): this approximation gives satisfactory results for all high-temperature superconductors with large but finite values of κ , typically $50 < \kappa < 100$.

In this case, the Ginzburg–Landau problem decouples and we have

$$\begin{cases} 0 = (-\mathbf{i}\nabla - \mathbf{A})^2 \psi - \psi(1 - |\psi|^2) & \text{in } \Omega, \\ 0 = \mathbf{n} \cdot (-\mathbf{i}\nabla - \mathbf{A})\psi & \text{on } \partial\Omega, \end{cases} \quad (2.2)$$

where $\mathbf{A} = \mathbf{A}(\mathbf{H}_0)$ is given by the relations

$$\begin{cases} \nabla \times (\nabla \times \mathbf{A}) = 0 & \text{in } \Omega, \\ \mathbf{n} \times (\nabla \times \mathbf{A}) = \mathbf{n} \times \mathbf{H}_0 & \text{on } \partial\Omega. \end{cases} \quad (2.3)$$

Since for this decoupled system there are no magnetization effects, the magnetic fields \mathbf{H}_0 and \mathbf{B} coincide.

Since the sample's width scales with ξ , the large- κ limit $\lambda \gg \xi$ means that the magnetic field \mathbf{A} penetrates the whole sample, independently of ψ .

In passing, we note that Equation (2.2) does not coincide with the so-called *Complex Ginzburg–Landau equation* (see [6] and references therein).

In the present paper, we consider a two-dimensional square sample

$$\Omega = \Omega_d := \{(x, y, z) \in \mathbb{R}^3 : (x, y) \in (-d/2, d/2)^2, z = 0\}, \quad d \in \mathbb{R}^+,$$

subject to a perpendicular, homogeneous magnetic field $\mathbf{H}_0 = (0, 0, \mu)^\top$, $\mu \in \mathbb{R}$. From (2.3) we can derive an expression for the induced vector potential

$$\mathbf{A}(x, y; \mu) = (A_x(x, y; \mu), A_y(x, y; \mu))^\top := \frac{1}{2}(-\mu y, \mu x)^\top, \quad (2.4)$$

where we have deliberately omitted the third component.

In conclusion, we will consider the following boundary-value problem with X_d being the natural energy space over Ω_d associated with the Gibbs energy (2.1) and Y_d its dual space. The equations are

$$\begin{aligned} \mathcal{GL}(\psi; \mu) : X_d \times \mathbb{R} &\rightarrow Y_d, \\ 0 = \mathcal{GL}(\psi; \mu) &:= \begin{cases} (-\mathbf{i}\nabla - \mathbf{A}(\mu))^2 \psi - \psi(1 - |\psi|^2) & \text{on } \Omega_d, \\ \mathbf{n} \cdot (-\mathbf{i}\nabla - \mathbf{A}(\mu))\psi & \text{on } \partial\Omega_d, \end{cases} \end{aligned} \quad (2.5)$$

where $\mathbf{A}(\mu)$ is given by (2.4), with the parameters $\mu \in \mathbb{R}$, $d \in \mathbb{R}^+$ and with the boundary conditions given in the sense of traces. To shorten the notation, the dependence of \mathbf{A} on μ will often not be made explicit in the remainder of the text.

Note that, because Ω_d is convex and $\mathbf{A} \in C^\infty(\bar{\Omega})$, solutions in the natural energy space immediately have higher regularity [8] and in fact coincide with the classical strong solutions in $C^2(\Omega) \cap C^1(\bar{\Omega})$.

Symmetries. As mentioned in Section 1, symmetries play an important role in the bifurcations scenario of our problem. The Ginzburg–Landau system for extreme type-II superconductors, (2.5), is left invariant by the action of the circle group S^1 ,

$$\theta_\eta : \psi \mapsto \psi \exp(\mathbf{i}\eta), \quad \eta \in [0, 2\pi). \quad (2.6)$$

The circle-group symmetry is also referred to as *phase symmetry*.

In addition, $\mathcal{GL}(\psi; \mu)$ is invariant under rotations by $\pi/2$

$$\rho : \psi(x, y) \mapsto \psi(-y, x) \quad (2.7)$$

and conjugated mirroring along the y -axis,

$$\sigma : \psi(x, y) \mapsto \overline{\psi(-x, y)}. \quad (2.8)$$

Note that, up to conjugation in σ , these are the classical group actions that generate the D_4 symmetry group of the square. In fact, the group generated by ρ and σ is isomorphic to D_4 . Even though symmetries of the Ginzburg–Landau problem have been considered before [15], the analysis was limited only to a linearization of the Ginzburg–Landau operator in the presence of rotations (2.7); in our case, we will consider the nonlinear problem and account also for conjugate reflections (2.8).

In conclusion, the relevant symmetry group for our problem is generated by the actions (2.6)–(2.8),

$$\Gamma := \langle \theta_\eta, \rho, \sigma \rangle \cong S^1 \times D_4.$$

We refer to the reader to Section 4, where we will explain how to factor out the continuous S^1 -symmetry that induces a singularity in the boundary-value problem associated with $\mathcal{GL}(\psi; \mu)$, and we conclude this section by showing in Figure 2.1 a few examples of patterns computed via numerical continuation. The Ginzburg–Landau

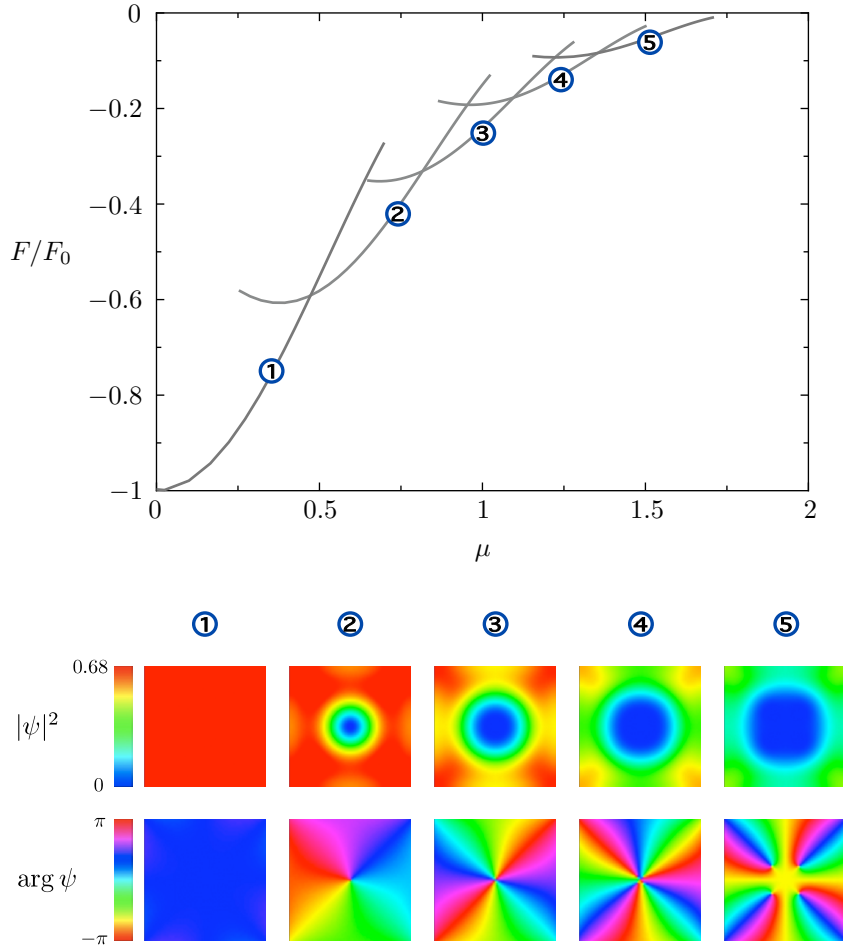


Fig. 2.1: Several families of stable solution branches of the Ginzburg–Landau equation (2.5) as a function of the bifurcation parameter μ , the intensity of the applied magnetic field. The results, obtained via numerical continuation, are computed for a square of side length $d = 5.5$. Top: On the vertical axis, we plot a measure of the Gibbs energy of the states (see remark 2 on page 17). We observe a cascade of instabilities similar to the one shown in the center panel of Figure 1.2, albeit the number of solution branches is larger in the latter diagram. As we will see in Section 6.2, the number of stable primary branches increases with the domain size d (the computations in the center panel of Figure 1.2 are for $d = 7.1$). Bottom: Selected stable patterns along the branches. Vortices are characterized by a localized region of low supercurrent density (blue in the pictures), as well as a $2\pi k$ -phase change in $\arg \psi$, where k is the *multiplicity* of the vortex. For higher values of μ , vortices with higher multiplicities are found: pattern 3, for instance, has a $2 \times 2\pi$ phase change, it is a *giant vortex* with multiplicity 2. All patterns shown have full D_4 -symmetry and we expect to interpret the diagram in terms of symmetry-breaking bifurcations.

problem (2.5) possesses two trivial solutions: $\mathcal{GL}(0; \mu) = 0$ for all $\mu \in \mathbb{R}$ (the normal state) and $\mathcal{GL}(1; 0) = 0$ (the homogeneously superconducting state). As expected, we find branches of nontrivial stable D_4 -symmetric solutions arranged in a characteristic cascade, in agreement with the results obtained by direct numerical simulations where the parameter μ is varied quasi-statically (see Figure 1.2).

3. The Jacobian operator. The patterns shown in Figure 2.1 were computed as regular zeros of a nonlinear system of equations derived from the Ginzburg–Landau problem (2.5). The solutions were found via Newton-Krylov iterations, that require the specification of the action of the Jacobian associated with $\mathcal{GL}(\psi; \mu)$ (see [30] for details on iterative linear solvers). Even though there were previous attempts to solve (2.5) with a modified Newton’s method [28], those implementations did not retain second-order convergence. Before deriving explicitly the regularization procedure that allowed us to compute the superconducting patterns, we introduce in this section the Jacobian operator $\mathcal{J}(\psi; \mu)$ associated with $\mathcal{GL}(\psi; \mu)$, and prove its self-adjointness with respect to a suitably-defined inner product in X_d .

For a given $d \in \mathbb{R}^+$, $\mu \in \mathbb{R}$, and $\psi, \delta\psi \in X_d$, let us consider

$$\begin{aligned} & \mathcal{GL}(\psi + \delta\psi; \mu) - \mathcal{GL}(\psi; \mu) \\ &= \left[(-i\nabla - \mathbf{A})^2(\psi + \delta\psi) - (\psi + \delta\psi) \left(1 - \overline{(\psi + \delta\psi)}(\psi + \delta\psi) \right) \right] \\ & \quad - \left[(-i\nabla - \mathbf{A})^2\psi - \psi \left(1 - \overline{\psi}\psi \right) \right] \\ &= (-i\nabla - \mathbf{A})^2\delta\psi + \psi \left(\overline{\psi}\delta\psi + \psi\overline{\delta\psi} + \overline{\delta\psi}\delta\psi \right) \\ & \quad - \delta\psi \left(1 - \overline{\psi}\psi \right) \\ & \quad + \delta\psi \left(\overline{\psi}\delta\psi + \psi\overline{\delta\psi} + \overline{\delta\psi}\delta\psi \right). \end{aligned}$$

Neglecting higher-order terms in $\delta\psi$, we obtain the Jacobian operator

$$\begin{aligned} \mathcal{J}(\psi; \mu) : X_d &\rightarrow Y_d, \\ \mathcal{J}(\psi; \mu)\varphi &:= \left((-i\nabla - \mathbf{A})^2 - 1 + 2|\psi|^2 \right) \varphi + \psi^2\overline{\varphi}. \end{aligned} \tag{3.1}$$

Note that $\mathcal{J}(\psi; \mu)$ is indeed linear when defined over X_d and Y_d as \mathbb{R} -vector spaces.

We are now going to prove that the Jacobian operator (3.1) is self-adjoint with respect to the inner product

$$\langle \cdot, \cdot \rangle_{\mathbb{R}} := \Re \langle \cdot, \cdot \rangle_{L_{\mathbb{C}}^2(\Omega)}. \tag{3.2}$$

This property allows us to employ standard methods for symmetric linear systems such as the conjugate gradient or the minimal residual method (using this inner product) to invert the Jacobian at each Newton iteration. Note that $\langle \cdot, \cdot \rangle_{\mathbb{R}}$ coincides with the natural inner product in $(L_{\mathbb{R}}^2(\Omega))^2$, which is isomorphic to $L_{\mathbb{C}}^2(\Omega)$, because for any given pair $\phi, \psi \in L_{\mathbb{C}}^2(\Omega)$, one has

$$\left\langle \begin{pmatrix} \Re\phi \\ \Im\phi \end{pmatrix}, \begin{pmatrix} \Re\psi \\ \Im\psi \end{pmatrix} \right\rangle_{(L_{\mathbb{R}}^2(\Omega))^2} = \langle \Re\phi, \Re\psi \rangle_{L_{\mathbb{R}}^2(\Omega)} + \langle \Im\phi, \Im\psi \rangle_{L_{\mathbb{R}}^2(\Omega)} = \langle \phi, \psi \rangle_{\mathbb{R}}.$$

The following lemma gives insight into the adjoint of a linear operator of the form (3.1). The lemma is formulated for general Hilbert spaces, and we will use it

for $H = L^2_{\mathbb{C}}(\Omega)$; in our case, the operation C mentioned below will be the pointwise complex conjugation.

LEMMA 3.1. *Let H be a Hilbert-space with inner product $\langle \cdot, \cdot \rangle_H$ and let there be an operation $C : H \rightarrow H$ such that*

$$C(\alpha x) = \alpha C(x) \quad \text{for all } \alpha \in \mathbb{R}, x \in H \quad (3.3)$$

$$\Re \langle C(x), y \rangle_H = \Re \langle x, C(y) \rangle_H \quad \text{for all } x, y \in H. \quad (3.4)$$

Let $\mathcal{L}_1, \mathcal{L}_2 : H \rightarrow H$ be linear operators. For every $x \in H$, let

$$\mathcal{L}x := \mathcal{L}_1x + \mathcal{L}_2C(x).$$

Then \mathcal{L} is a linear operator on H as \mathbb{R} -vector space, and its adjoint \mathcal{L}^* with respect to the inner product $\langle \cdot, \cdot \rangle_{\mathbb{R}} := \Re \langle \cdot, \cdot \rangle_H$ is given by

$$\mathcal{L}^*x := \mathcal{L}_1^*x + C(\mathcal{L}_2^*x),$$

where $\mathcal{L}_1^*, \mathcal{L}_2^*$ are the adjoint operators in H of $\mathcal{L}_1, \mathcal{L}_2$, respectively.

Proof. Let $x, y \in H$, and consider

$$\langle x, \mathcal{L}y \rangle_{\mathbb{R}} = \Re \langle x, \mathcal{L}_1y + \mathcal{L}_2C(y) \rangle_H = \Re \langle x, \mathcal{L}_1y \rangle_H + \Re \langle x, \mathcal{L}_2C(y) \rangle_H.$$

Using the operator adjoints $\mathcal{L}_1^*, \mathcal{L}_2^*$, we get

$$\begin{aligned} \langle x, \mathcal{L}y \rangle_{\mathbb{R}} &= \Re \langle \mathcal{L}_1^*x, y \rangle_H + \Re \langle \mathcal{L}_2^*x, C(y) \rangle \\ &= \Re \langle \mathcal{L}_1^*x, y \rangle_H + \Re \langle C(\mathcal{L}_2^*x), y \rangle = \langle \mathcal{L}_1^*x + C(\mathcal{L}_2^*x), y \rangle_{\mathbb{R}} = \langle \mathcal{L}^*x, y \rangle_{\mathbb{R}}. \end{aligned}$$

□

LEMMA 3.2. *Let $\mathbf{A}(\mu) \in C^1_{\mathbb{R}^n}(\Omega)$, $n \in \{2, 3\}$. The kinetic energy operator*

$$\begin{aligned} \mathcal{K}(\mu) : X_d &\rightarrow Y_d, \\ \mathcal{K}(\mu)\varphi &:= \begin{cases} (-\mathbf{i}\nabla - \mathbf{A})^2\varphi, & \text{in } \Omega_d \\ \mathbf{n} \cdot (-\mathbf{i}\nabla - \mathbf{A})\varphi, & \text{on } \partial\Omega_d \end{cases} \end{aligned} \quad (3.5)$$

is self-adjoint with respect to the inner product $\langle \cdot, \cdot \rangle_{L^2_{\mathbb{C}}(\Omega_d)}$ over the subspace $X_d^0 \subseteq X_d$ with $\mathbf{n} \cdot (-\mathbf{i}\nabla - \mathbf{A})\varphi = 0$.

Proof. This result immediately derives from the fact that

$$\int_{\Omega} \overline{\psi} (-\mathbf{i}\nabla - \mathbf{A})^2\varphi \, d\Omega = \int_{\Omega} \overline{(-\mathbf{i}\nabla - \mathbf{A})\psi} (-\mathbf{i}\nabla - \mathbf{A})\varphi \, d\Omega - \mathbf{i} \int_{\partial\Omega} \overline{\psi} \mathbf{n} \cdot (-\mathbf{i}\nabla - \mathbf{A})\varphi \quad (3.6)$$

for all $\psi \in L^2_{\mathbb{C}}(\Omega_d)$, $\varphi \in X_d$, see [7]. □

COROLLARY 3.3. *For any $\psi \in X_d$ and $\mathbf{A}(\mu) \in C^1_{\mathbb{R}^n}(\Omega)$, the Jacobian operator $\mathcal{J}(\psi; \mu)$ defined in (3.1) is linear and self-adjoint over X_d^0 with respect to the inner product (3.2), $\langle \cdot, \cdot \rangle_{\mathbb{R}}$.*

Proof. By lemma 3.2, the operator of $\mathcal{J}_1(\psi; \mu) := ((-\mathbf{i}\nabla - \mathbf{A})^2 - 1 + 2|\psi|^2)$ defined over X_d^0 with respect to the $L^2_{\mathbb{C}}(\Omega_d)$ -inner product is self-adjoint. It can easily be checked that the adjoint operator of $\mathcal{J}_2(\psi)$, defined by $\mathcal{J}_2(\psi)\varphi = \psi^2\varphi$ for $\varphi \in X_d$, is given by $\mathcal{J}_2^*(\psi)\varphi = \overline{\psi^2}\varphi$. Also note that the complex conjugation fulfills the conditions (3.3). Application of lemma 3.1 then states that the adjoint of $\mathcal{J}(\psi; \mu) : X_d \rightarrow Y_d$ is given by

$$\mathcal{J}^*(\psi; \mu)\varphi = \mathcal{J}_1^*\varphi + \overline{\psi^2}\varphi = \mathcal{J}_1\varphi + \psi^2\overline{\varphi} = \mathcal{J}(\psi; \mu)\varphi$$

for all $\varphi \in X_d$, and thus $\mathcal{J}^*(\psi; \mu) = \mathcal{J}(\psi; \mu)$. □

4. Nullspace and regularization with a phase condition. As stated in the previous sections, our aim is to compute solutions to the Ginzburg–Landau problem (2.5) and continue them in the parameter μ . This can be done in principle by discretizing the Ginzburg–Landau operator and applying standard numerical continuation techniques.

However, as we have seen in Section 2, the boundary-value problem $\mathcal{GL}(\psi; \mu) = 0$ is invariant under the actions of the group $\Gamma = S^1 \times D_4$, and continuous symmetries (such as the phase symmetry determined by the circle group S^1) make the problem ill-posed. After discretization, this leads to numerical difficulties that make it principally impossible to compute accurate approximations to the original problem [18] (see Figure 5.1a).

This problem is usually met in computations of relative equilibria, which are time-dependent solutions whose temporal evolution is governed by a symmetry of the underlying differential equations. Typical examples are traveling waves (translational symmetries) and spiral waves (rotational symmetry). The continuous symmetry induces a zero eigenvalue in the Jacobian associated with the boundary-value problem, and it is therefore not straightforward to use Newton’s method to compute the desired pattern: each Newton iteration inverts the Jacobian evaluated at a given solution ψ and requires a regular linear operator.

A generic strategy to compute relative equilibria and to remove the singularity is to extend the boundary-value problem by introducing an additional scalar unknown and closing the system by means of a suitably-defined *phase condition* [11, 14, 33, 12]. The new boundary-value problem is well-posed, and therefore Newton’s method can find the solution and path-follow it as a function of the parameters. This regularization technique can be applied to the stationary patterns of the Ginzburg–Landau problem to factor out the action of the circle group S^1 . To the authors’ knowledge, the removal of the singularity for the Ginzburg–Landau system has not been considered in literature before. The regularization adopted here is an application of the framework proposed in [14].

In order to regularize the Ginzburg–Landau problem, we look at the action of $\xi_\eta \in \text{alg}(S^1)$, $\eta \in \mathbb{R}$, on a state ψ . Note that the exponential map of S^1 is given by $\exp : \text{alg}(S^1) \rightarrow S^1$, $\xi_\eta \mapsto \theta_\eta$, where θ_η is identified with the action $\theta_\eta \psi = e^{i\eta} \psi$ on a state ψ . This yields

$$\xi_\eta \psi = \left. \frac{d}{dt} \exp(\xi_\eta t) \psi \right|_{t=0} = \left. \frac{d}{dt} \theta_\eta t \psi \right|_{t=0} = \left. \frac{d}{dt} e^{i\eta t} \psi \right|_{t=0} = i\eta \psi,$$

and indeed the function $i\psi_s$ is in the nullspace of the Jacobian for a solution (ψ_s, μ_s) of (2.5):

$$\begin{aligned} \mathcal{J}(\psi_s; \mu_s)(i\psi_s) &= [(-i\nabla - \mathbf{A})^2 - 1 + 2|\psi_s|^2] (i\psi_s) - i\psi_s^2 \overline{\psi_s} \\ &= (1 - |\psi_s|^2) (i\psi_s) - i\psi_s + 2i\overline{\psi_s} \psi_s^2 - i\psi_s^2 \overline{\psi_s} = 0. \end{aligned} \quad (4.1)$$

It is then possible to amend the Ginzburg–Landau problem and factor out the action of S^1 . To this end, for fixed μ , we compute (ψ, η) as a regular zero of the extended operator

$$\begin{aligned} \mathcal{GL}_p : X_d \times \text{alg}(S^1) &\longrightarrow Y_d \times \mathbb{R} \\ (\psi, \eta) &\longmapsto (\mathcal{GL}(\psi; \mu) - \xi_\eta \psi, \Phi(\psi - \psi_0)) \end{aligned}$$

where $\Phi: X_d \rightarrow \mathbb{R}$ is a suitable phase condition and ψ_0 a given reference state. In the Ginzburg–Landau setting, the natural choice is the functional

$$\Phi: X_d \longrightarrow \mathbb{R}, \quad \psi \longmapsto \Re\langle \mathfrak{i}\psi_0, \psi - \psi_0 \rangle \quad (4.2)$$

with a given reference state $\psi_0 \in L^2_{\mathbb{C}}(\Omega_d)$, subject to mild conditions (see corollary 4.1). Hence, instead of (2.5), we will consider the extended problem

$$0 = \mathcal{GL}_p(\psi, \eta; \mu) := \begin{pmatrix} \mathcal{GL}(\psi; \mu) - \mathfrak{i}\eta\psi \\ \Im(\langle \psi_0, \psi \rangle_{L^2_{\mathbb{C}}(\Omega_d)}) \end{pmatrix}. \quad (4.3)$$

REMARK 1. *The phase condition featuring in (4.3) is also a necessary condition for*

$$\min_{\chi \in \mathbb{R}} \|\psi_0 - \psi e^{\mathfrak{i}\chi}\|_{L^2_{\mathbb{C}}(\Omega_d)}^2.$$

This selects, out of all physically equivalent candidate solution states $\psi e^{\mathfrak{i}\chi}$, those two which are closest and furthest from ψ_0 in the $L^2_{\mathbb{C}}(\Omega_d)$ -norm.

If $\psi_s \in X_d$ is a solution of the original equations (2.5), then $(\exp(\mathfrak{i}\chi_s)\psi_s, 0)^T$ with $\chi_s := -\arg(\langle \psi_0, \psi_s \rangle_{L^2_{\mathbb{C}}(\Omega_d)})$ is a solution of (4.3) as well. The Jacobian operator corresponding to the extended problem (4.3) is

$$\begin{aligned} \mathcal{J}_p(\psi, \eta; \mu) : X_d \times \mathbb{R} &\rightarrow Y_d \times \mathbb{R}, \\ \mathcal{J}_p(\psi, \eta; \mu) \begin{pmatrix} \varphi \\ \nu \end{pmatrix} &= \begin{pmatrix} (\mathcal{J}(\psi; \mu) - \mathfrak{i}\eta)\varphi - \mathfrak{i}\psi\nu \\ \Im(\langle \psi_0, \varphi \rangle_{L^2_{\mathbb{C}}(\Omega_d)}) \end{pmatrix}. \end{aligned} \quad (4.4)$$

We expect that the dimension of the nullspace of the extended Jacobian (4.4) is lower than the one of $\mathcal{J}(\psi; \mu)$. This is guaranteed by Keller’s bordering lemma [29] if $\dim \ker \mathcal{J}(\psi; \mu) = 1$. However, in the case of the Ginzburg–Landau operator we will encounter degeneracies of higher order. In the appendix, we present a bordering lemma that can be applied in such cases (Lemma A.1) and that is used in the proof of the following corollary.

COROLLARY 4.1. *Let $(\psi_s, \mu_s) \in X_d \times \mathbb{R}$ be a solution of the original Ginzburg–Landau equations (2.5) with $\psi_s \neq 0$, and let $\psi_0 \in L^2_{\mathbb{C}}(\Omega_d)$ such that $\langle \psi_0, \psi_s \rangle_{L^2_{\mathbb{C}}(\Omega_d)} \neq 0$. Then*

$$\dim \ker \mathcal{J}_p(\psi_s; \mu_s) < \dim \ker \mathcal{J}(\psi_s; \mu_s).$$

Proof. The corollary is a direct consequence of lemma A.1 (page 27) so it suffices here to verify that it can be applied on $\mathcal{J}_p(\psi; \mu)$. First note that the phase condition $\Im(\langle \psi_0, \varphi \rangle_{L^2_{\mathbb{C}}(\Omega_d)})$ is a linear functional over the \mathbb{R} -vector space X_d . Furthermore, we have by (4.1) that $\text{span}\{\mathfrak{i}\psi_s\} \subseteq \ker \mathcal{J}(\psi_s; \mu_s)$. Evaluating the phase condition at $\mathfrak{i}\psi_s$ yields

$$\Im(\langle \psi_0, \mathfrak{i}\psi_s \rangle_{L^2_{\mathbb{C}}(\Omega_d)}) = \langle \psi_0, \psi_s \rangle_{L^2_{\mathbb{C}}(\Omega_d)} \neq 0$$

by assumption. Moreover, corollary 3.3 states that $\mathcal{J}(\psi_s; \mu_s) = \mathcal{J}^*(\psi_s; \mu_s)$ with respect to the inner product (3.2). From this, it follows that

$$\mathcal{R}(\mathcal{J}(\psi_s; \mu_s)) = \ker(\mathcal{J}^*(\psi_s; \mu_s))^{\perp} = \ker(\mathcal{J}(\psi_s; \mu_s))^{\perp},$$

so to show that $b = -\mathbf{i}\psi_s \notin \mathcal{R}(\mathcal{J})$ it suffices to show that b is not orthogonal to all of $\ker(\mathcal{J}(\psi_s; \mu_s))$ with respect to the inner product (3.2). This holds true for $\psi_s \neq 0$ since

$$\langle \mathbf{i}\psi_s, \mathbf{i}\psi_s \rangle_{\mathbb{R}} = \Re \langle \psi_s, \psi_s \rangle_{L^2_{\mathbb{C}}(\Omega_d)} = \|\psi_s\|_{L^2_{\mathbb{C}}(\Omega_d)}^2 \neq 0.$$

Thus, all conditions of lemma A.1 are fulfilled and its application to $\mathcal{J}_p(\psi; \mu)$ concludes the proof. \square

In the remainder of this section, we show that the extended operator retains the symmetries of the Ginzburg–Landau system.

Symmetries of the extended system. Given $\gamma \in \Gamma$, the symmetries $\tilde{\gamma}$ of the extended system are defined to act

$$\tilde{\gamma} \begin{pmatrix} \psi \\ \eta \end{pmatrix} := \begin{pmatrix} \gamma\psi \\ \eta \end{pmatrix}. \quad (4.5)$$

LEMMA 4.2. *The extended system (4.3) is equivariant exactly under all actions in Γ that leave ψ_0 invariant, i.e., $\tilde{\Gamma} = \Sigma_{\psi_0} \cap \Gamma$.*

Proof. We have to prove equivariance only for the generators $\tilde{\rho}, \tilde{\sigma} \in \tilde{\Gamma}$. For a given $\gamma \in \Sigma_{\psi_0} \cap \Gamma$, it has to be shown that

$$\left(\gamma [\mathcal{GL}(\psi) - \mathbf{i}\eta\psi] \right) = \tilde{\gamma} \mathcal{GL}_p(\psi, \eta) \stackrel{!}{=} \mathcal{GL}_p(\tilde{\gamma}(\psi, \eta)) = \left(\mathcal{GL}(\gamma\psi) - \mathbf{i}\eta(\gamma\psi) \right),$$

which holds obviously true for the first component, owing to the Γ -invariance of \mathcal{GL} . As for the second component, we have

$$\Im(\langle \psi_0, \psi \rangle_{L^2_{\mathbb{C}}(\Omega_d)}) \stackrel{!}{=} \Im(\langle \psi_0, \gamma\psi \rangle_{L^2_{\mathbb{C}}(\Omega_d)}) = \Im \left(\int_{\Omega} \bar{\psi}_0(\gamma\psi) \, d\Omega \right).$$

After a suitable change of variables, this is equivalent to show that

$$\Im(\langle \psi_0, \psi \rangle_{L^2_{\mathbb{C}}(\Omega_d)}) \stackrel{!}{=} \Im \left(\int_{\Omega} (\gamma^{-1}\bar{\psi}_0)\psi \det \vartheta_{\gamma} \, d\Omega \right) \quad \forall \psi \in L^2_{\mathbb{C}}(\Omega) \quad (4.6)$$

holds exactly for all $\gamma \in \Sigma_{\psi_0} \cap \Gamma$.

Firstly, let us show this equivalence for the cyclic subgroup $C_4 \preceq \Sigma_{\psi_0}$. Given $\gamma \in C_4$ (and thus $\gamma\psi_0 = \psi_0$, $\det \vartheta_{\gamma} = 1$), equation (4.6) obviously holds true. On the other hand, let us assume that equation (4.6) is valid and let us take a sequence of Dirac- δ functions centered at (x_0, y_0) , $\psi^{(l)} = \delta^l_{(x_0, y_0)}$. Then

$$\begin{aligned} \Im(\bar{\psi}_0(x_0, y_0)) &= \lim_{l \rightarrow \infty} \Im \left(\int_{\Omega} \bar{\psi}_0 \psi^{(l)} \, d\Omega \right) \stackrel{!}{=} \\ &= \lim_{l \rightarrow \infty} \Im \left(\int_{\Omega} \gamma^{-1}\bar{\psi}_0 \psi^{(l)} \, d\Omega \right) = \Im((\gamma^{-1}\bar{\psi}_0)(x_0, y_0)) \end{aligned}$$

Since this can be done for any $(x_0, y_0) \in \Omega \cup \partial\Omega$, we have $\Im(\psi_0) \in C_4$. The same result is obtained for $\Re(\psi_0)$ by taking $\psi^{(l)} = \mathbf{i}\delta^l_{(x_0, y_0)}$. We conclude that $\Sigma_{\psi_0} \supseteq C_4$ is also necessary for (4.6) to hold.

The very same arguments can be applied to the conjugate reflection σ , noting that $\det \vartheta_{\sigma} = -1$, and that the action of σ changes the sign of the expression. \square

The choice of ψ_0 must hence be such that it eliminates the phase invariance (according to corollary 4.1), and that it preserves the other symmetries of the system (according to lemma 4.2). The first condition is equivalent to demanding $0 \neq \langle \psi_0, \psi_s \rangle$ which indeed is a rather mild condition that will be fulfilled, for instance, by $\psi_0 \equiv 1$ for most scenarios considered later. Note that it is also possible to update ψ_0 in each Newton step to the current guess $\psi^{(k)}$: For a solution ψ_s , let $\psi_s = \psi^{(k)} + e^{(k)}$; we have

$$\langle \psi^{(k)}, \psi_s \rangle = \|\psi_s\|_{L^2_{\mathbb{C}}(\Omega_d)}^2 + \langle e^{(k)}, \psi \rangle,$$

which is guaranteed to be nonzero for sufficiently small $e^{(k)}$ if $\psi_s \neq 0$. Note that intermediate Newton steps might not exactly preserve the symmetries of the system, but the symmetry breaking is weak in the sense that symmetry is preserved at convergence, and will not do harm [27].

5. The discretized system. An important property of the full Ginzburg–Landau equations is its *gauge invariance*, a generalization of the phase symmetry (2.6) to the case where \mathbf{A} is not fixed (see section 3.1 in [21]). While the reduced invariance with fixed \mathbf{A} is preserved under all consistent pointwise discretizations of the Ginzburg–Landau equations [20, 22, 28], ordinary finite-difference discretizations lead to systems that are gauge invariant only up to $O(h)$, where h is the grid spacing. It is thus customary to reformulate the equations using techniques from lattice gauge theory. For the convenience of the reader, the new system will be presented in this section. We also show that, for appropriate phase conditions, all the symmetries are preserved in the extended discretized system.

5.1. Formulation with link variables. Let us consider the functions

$$\begin{aligned} U_x(x, y) &:= \exp\left(-\mathbf{i} \int_{x_0}^x A_x(\xi, y) \, d\xi\right), \\ U_y(x, y) &:= \exp\left(-\mathbf{i} \int_{y_0}^y A_y(x, \nu) \, d\nu\right), \end{aligned}$$

with arbitrary, fixed $x_0, y_0 \in \mathbb{R}$. It can be checked easily that

$$\sum_{\nu \in \{x, y\}} -\overline{U_\nu(x, y)} \frac{\partial^2}{\partial \nu^2} (U_\nu \psi) = (-\mathbf{i} \nabla - \mathbf{A})^2 \psi - \mathbf{i} (\nabla \cdot \mathbf{A}) \psi.$$

The Ginzburg–Landau equations (2.2) can then be written as

$$\begin{cases} 0 = - \sum_{\nu \in \{x, y\}} \overline{U_\nu \psi} \frac{\partial^2}{\partial \nu^2} (U_\nu \psi) - \overline{\psi} \psi (1 - \overline{\psi} \psi) & \text{in } \Omega, \\ 0 = \mathbf{n} \cdot \begin{pmatrix} \overline{U_x \psi} \frac{\partial}{\partial x} (U_x \psi) \\ \overline{U_y \psi} \frac{\partial}{\partial y} (U_y \psi) \end{pmatrix} & \text{on } \partial\Omega. \end{cases} \quad (5.1)$$

U_ν only appears in the product $U_\nu \psi$ which guarantees preservation of full gauge invariance [21].

5.1.1. Discretization. Let $N > 0$, for simplicity even, $h = d/N$, and let $\Omega_h = \{h \cdot (i, j) \mid -N/2 \leq i \leq N/2, -N/2 \leq j \leq N/2\}$ be a uniform grid on Ω_d . Furthermore,

let us consider the discretization $\psi^{(h)} \in X_h = \mathbb{C}^{(N+1) \times (N+1)}$. The ordinary five-point discretization of (5.1) with centered finite differences on the boundaries is given by

$$0 = \mathcal{GL}^{(h)}(\psi^{(h)}; \mu) := \left(D_{xx} \psi^{(h)} \right)_{i,j} + \left(D_{yy} \psi^{(h)} \right)_{i,j} - \psi_{i,j}^{(h)} \left(1 - \overline{\psi_{i,j}^{(h)}} \psi_{i,j}^{(h)} \right) \\ \forall i, j \in \{-N/2, \dots, N/2\} \quad (5.2)$$

where the finite-difference operator D_{xx} is defined by

$$\left(D_{xx} \psi^{(h)} \right)_{i,j} := \begin{cases} h^{-2} \left(2\psi_{i,j}^{(h)} - 2(U_x^{(h)})_{i-1,j} \psi_{i-1,j}^{(h)} \right) & \text{for } i = N/2, \\ h^{-2} \left(-(U_x^{(h)})_{i+1,j} \psi_{i+1,j}^{(h)} + 2\psi_{i,j}^{(h)} - (U_x^{(h)})_{i-1,j} \psi_{i-1,j}^{(h)} \right) & \text{for } -\frac{N}{2} < i < \frac{N}{2}, \\ h^{-2} \left(-2(U_x^{(h)})_{i+1,j} \psi_{i+1,j}^{(h)} + 2\psi_{i,j}^{(h)} \right) & \text{for } i = -N/2, \end{cases}$$

and likewise for $D_{yy} \psi^{(h)}$, with unknown $\psi^{(h)} \in X_h$, where

$$(U_x^{(h)})_{i\pm 1,j} = \exp(-i I_{x_i}^{x_{i\pm 1}}(A_x(\cdot, y_j))) + O(h^p)$$

with $I_{x_i}^{x_{i\pm 1}}(A_x(\cdot, y_j)) \approx \int_{x_i}^{x_{i\pm 1}} A_x(\xi, y_j) d\xi$, and likewise for $(U_y^{(h)})_{x,j\pm 1}$. The order p of the approximation depends on the quadrature method in use. It is easy to verify that the discretization (5.2) has order of consistency $\min\{2, p-2\}$.

The discrete Jacobian operator $\mathcal{J}^{(h)}$ is defined similarly as

$$\mathcal{J}^{(h)}(\psi^{(h)}; \mu) : X_h \rightarrow X_h, \\ \left(\mathcal{J}^{(h)}(\psi^{(h)}; \mu) \varphi^{(h)} \right)_{i,j} := \left(D_{xx} \psi^{(h)} \right)_{i,j} + \left(D_{yy} \psi^{(h)} \right)_{i,j} - \varphi_{i,j}^{(h)} + 2 \left| \psi_{i,j}^{(h)} \right|^2 \varphi_{i,j}^{(h)} \\ + \left(\psi_{i,j}^{(h)} \right)^2 \overline{\varphi_{i,j}^{(h)}} \quad (5.3)$$

and it is self-adjoint with respect to the scalar product $\Re\langle \cdot, \cdot \rangle_{\mathbb{C}}$. This is a consequence of lemma 3.1 upon realizing that the operators D_{xx} and D_{yy} are both self-adjoint with respect to the inner product $\langle \cdot, \cdot \rangle_{\mathbb{C}}$ in $\mathbb{C}^{(N+1) \times (N+1)}$. A consequence of this is that all eigenvalues of the operator (5.3) are real-valued.

5.1.2. Symmetries of the discretized system. Now that the structure of the discretized operator is described, we review the symmetries of the associated boundary-value problem. Many of the results in this section can be borrowed from Section 4 on the continuous problem with little modification. For example, the discretized system (5.2) is invariant under

$$\left(\theta_{\eta}^{(h)} \psi^{(h)} \right)_{i,j} := \exp(i\eta) \psi_{i,j}^{(h)}$$

pointwise for each $\eta \in [0, 2\pi)$. Let further the discrete symmetry operators ρ and σ be defined by

$$\left(\rho^{(h)} \psi^{(h)} \right)_{i,j} := \psi_{j,-i}^{(h)}, \quad \left(\sigma^{(h)} \psi^{(h)} \right)_{i,j} := \overline{\psi_{-i,j}^{(h)}}. \quad (5.4)$$

It can easily be shown that the discretized system (5.2) is invariant under these actions.

Just like in the continuous case (4.1), the discrete phase invariance induces a nontrivial nullspace of $\mathcal{J}^{(h)}$:

$$\begin{aligned}
\left(\mathcal{J}^{(h)}(\psi^{(h)}; \mu) \mathfrak{i}\psi^{(h)}\right)_{i,j} &= \mathfrak{i} \left(D_{xx}\psi^{(h)}\right)_{i,j} + \mathfrak{i} \left(D_{yy}\psi^{(h)}\right)_{i,j} - \mathfrak{i}\psi_{i,j}^{(h)} + 2\mathfrak{i} \left|\psi_{i,j}^{(h)}\right|^2 \psi_{i,j}^{(h)} \\
&\quad - \mathfrak{i} \left(\psi_{i,j}^{(h)}\right)^2 \overline{\psi_{i,j}^{(h)}} \\
&= \mathfrak{i}\psi_{i,j}^{(h)} \left(1 - \overline{\psi_{i,j}^{(h)}}\psi_{i,j}^{(h)}\right) - \mathfrak{i}\psi_{i,j}^{(h)} + \mathfrak{i} \left|\psi_{i,j}^{(h)}\right|^2 \psi_{i,j}^{(h)} \\
&= 0.
\end{aligned} \tag{5.5}$$

and hence $\mathfrak{i}\psi_{i,j}^{(h)} \in \ker \mathcal{J}^{(h)}(\psi_s^{(h)}; \mu_s)$. This makes it impossible to treat the system (5.2) with generic linear solvers at a solution $\psi_s^{(h)}$, as the system is then exactly singular. In the neighborhood of $\psi_s^{(h)}$, the system will have a large condition number, making round-off errors dominate the update term [18] which in turn flaws the next Newton step. This phenomenon is illustrated in Figure 5.1a.

As suggested in section 4, we will avoid the singularity of the Jacobian by using a phase condition, which in its discretized form reads

$$I^{(h)}(\psi_0^{(h)}, \psi^{(h)}) := \Im \left(\sum_{i=-N/2}^{N/2} w_i h \sum_{j=-N/2}^{N/2} w_j h \overline{\left(\psi_0^{(h)}\right)_{i,j}} \psi_{i,j}^{(h)} \right), \tag{5.6}$$

where $\psi_0^{(h)} \in X_h$ is a given reference state, and

$$w_i = \begin{cases} 1 & \text{for } -N/2 < i < N/2, \\ \frac{1}{2} & \text{for } i \in \{-N/2, N/2\}. \end{cases}$$

The discretized version of the extended system is then

$$0 = \mathcal{GL}_p^{(h)}(\psi^{(h)}, \eta; \mu) := \begin{pmatrix} \mathcal{GL}^{(h)}(\psi^{(h)}; \mu) - \mathfrak{i}\eta\psi^{(h)} \\ I^{(h)}(\psi_0^{(h)}, \psi^{(h)}) \end{pmatrix}, \tag{5.7}$$

and the symmetry operations for this extended system can be defined just like in (4.5).

Parallel to (4.4), the discrete extended Jacobian operator $\mathcal{J}^{(h)}$ is

$$\begin{aligned}
\mathcal{J}_p^{(h)}(\psi^{(h)}; \eta; \mu) : X_h \times \mathbb{R} &\rightarrow X_h \times \mathbb{R}, \\
\left(\mathcal{J}_p^{(h)}(\psi^{(h)}; \eta; \mu) \begin{pmatrix} \varphi^{(h)} \\ \nu \end{pmatrix}\right)_{i,j} &:= \begin{pmatrix} \left(\mathcal{J}^{(h)}(\psi^{(h)}; \mu) - \mathfrak{i}\eta\right)\varphi^{(h)} - \mathfrak{i}\psi^{(h)}\nu \\ I^{(h)}(\psi_0^{(h)}, \varphi^{(h)}) \end{pmatrix}
\end{aligned} \tag{5.8}$$

The following two statements are the discrete versions of the lemmas 4.1 and 4.2.

COROLLARY 5.1. *Let $(\psi_s^{(h)}, \mu_s) \in X_h \times \mathbb{R}$ be a solution of the original discretized Ginzburg–Landau equations (5.2) with $\psi_s^{(h)} \neq 0$, and let $\psi_0^{(h)} \in X_h$ such that $\langle \psi_0^{(h)}, \psi_s^{(h)} \rangle_{\mathbb{C}} \neq 0$. Then*

$$\dim \ker \mathcal{J}_p^{(h)}(\psi_s^{(h)}; \mu_s) < \dim \ker \mathcal{J}^{(h)}(\psi_s^{(h)}; \mu_s).$$

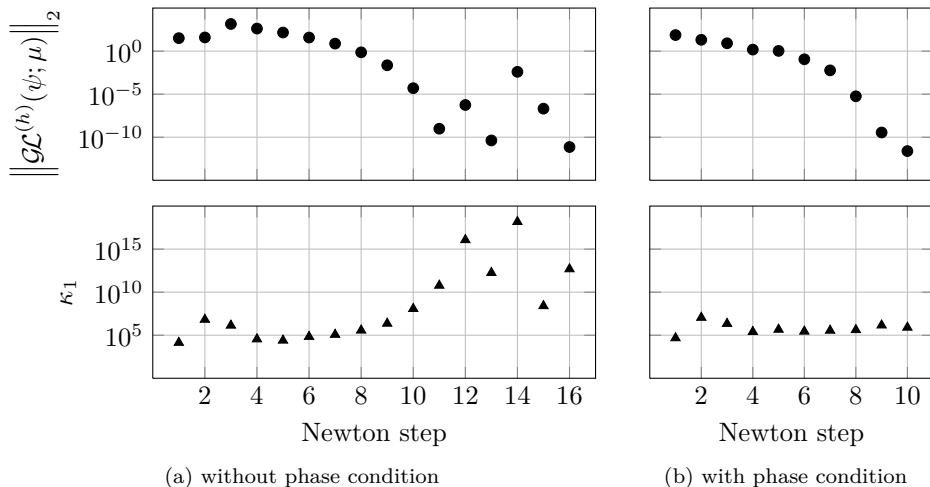


Fig. 5.1: The residual of the Newton iterations and the condition number κ_1 of the associated linear system in the 1-norm. (a) Here, the linear Jacobian systems are solved using Gaussian elimination and deliver flawed Newton updates as the condition number increases. This is a principle problem and it is not limited to Gaussian elimination. (b) The regularization removes the singularity and this leads to bounded condition numbers. The linear systems can then be solved accurately.

Proof. The proof runs parallel to the one of corollary 4.1, using the discrete inner product $\Re\langle \cdot, \cdot \rangle_{\mathbb{C}}$. \square

LEMMA 5.2. *The extended equations (5.7) are equivariant exactly under $\Sigma_{\psi_0^{(h)}} \cap \Gamma^{(h)}$.*

Proof. Again, the proof is essentially parallel to the one of lemma 4.2; instead of series of Dirac- δ function $\delta_{(x_0, y_0)}$, we can use their discrete equivalents

$$\varphi_{i,j}^{(h)} := \begin{cases} 1 & \text{for } i = i_0, j = j_0 \\ 0 & \text{otherwise} \end{cases}, \quad \tilde{\varphi}_{i,j}^{(h)} := \mathbb{i} \varphi_{i,j}^{(h)}.$$

\square

6. Numerical results. Using the framework presented in the previous sections, it is possible to solve the Ginzburg–Landau equations numerically for any given parameter μ (the strength of the applied magnetic field) and d (the edge length of the sample). As discussed in Section 1, the intensity of the applied magnetic field, can be tuned experimentally, and it is thus interesting to explore the bifurcation scenario as this parameter is varied.

Because of the symmetries of the Ginzburg–Landau system posed on the square, we expect symmetry-breaking bifurcations to arise. As described in Section 4, the extended system (4.3) does not bear the continuous S^1 -symmetry such that the relevant symmetry group for our computations is D_4 .

Symmetry-breaking bifurcations in D_4 are well known [27, 24]. We recall here that, in our case, the group generators are ρ , the rotation by $\pi/2$ (see equation (2.7)),

and σ , the conjugated mirroring along the y -axis (see equation (2.8)). We expect that symmetry-breaking bifurcations will occur when critical eigenvalues become unstable with (algebraic and geometric) multiplicity either 1 or 2. With a simple unstable eigenvalue, one should expect either a symmetry-preserving turning point or a pitchfork bifurcation with branches corresponding to the four one-dimensional irreducible representations of D_4 . With an eigenvalue of multiplicity 2 crossing the origin, two families of branches emerge from the bifurcation point, corresponding to the conjugacy classes of the D_4 isotropy subgroups $\langle \rho \rangle$ and $\langle \sigma\rho \rangle$, respectively.

In the present section, the parameter μ will be varied for two different domain sizes d . The simplest nontrivial example of symmetry-breaking bifurcation occurs for small domain sizes, so we have deliberately chosen $d = 3.0$, a domain size that is just enough to host a single vortex. Subsequently, we study the case $d = 5.5$, for which the bifurcation scenario becomes increasingly more involved.

The bifurcation diagrams are traced via standard numerical continuation methods [31]. The technical implementation is based on the Trilinos project [26] and exploits the sparse structure of the discrete Jacobian operator (5.3) as well as its properties, as outlined in Section 3.

In the remainder of this section, we will denote solution branches (and relative patterns) alphabetically and bifurcation points with numerals.

REMARK 2. *Unless otherwise stated, the bifurcation diagrams are plotted in terms of the expression*

$$F(\psi, \mu) := F_{max}^{-1} \xi \frac{|\alpha|^2}{\beta} \int_{\Omega} -|\psi|^2 + \frac{1}{2}|\psi|^4 + |-\mathbf{i}\nabla\psi - \mathbf{A}(\mu)\psi|^2 \, d\Omega \quad (6.1)$$

which is part of the Gibbs energy (2.1). This is in accordance to what is usually done in the physics literature. Applying (3.6) in the case $\psi \in X_d$, we obtain

$$F(\psi, \mu) = F_{max}^{-1} \xi \frac{|\alpha|^2}{\beta} \left[\int_{\Omega} -|\psi|^2 + \frac{1}{2}|\psi|^4 + \int_{\Omega} \bar{\psi}(-\mathbf{i}\nabla\psi - \mathbf{A}(\mu))^2\psi \, d\Omega \right].$$

Only solutions $\psi(\mu)$ of the Ginzburg–Landau equations (2.2) are considered, so that

$$\begin{aligned} F(\psi, \mu) &= F_{max}^{-1} \xi \frac{|\alpha|^2}{\beta} \left[\int_{\Omega} -|\psi|^2 + \frac{1}{2}|\psi|^4 + \int_{\Omega} \bar{\psi}\psi(1 - |\psi|^2) \, d\Omega \right] \\ &= -F_{max}^{-1} \xi \frac{|\alpha|^2}{2\beta} \int_{\Omega} |\psi|^4 \, d\Omega. \end{aligned}$$

Thus, computing the significant portion (6.1) of the Gibbs energy (2.1) effectively reduces to evaluating

$$F(\psi, \mu) = -|\Omega|^{-1} \int_{\Omega} |\psi|^4 \, d\Omega.$$

6.1. Small-sized system ($d = 3$). The first computed solution corresponds to a superconductor in the absence of a magnetic field, that is, $\mu = 0$; the system is in the homogeneous solution $\psi \equiv 1$ and it is said to be in a completely superconducting state. The solution has all the symmetries of the system (its isotropy subgroup is the full group D_4) and is stable as a global minimum of the free energy (2.1).

With the help of numerical continuation, a series of solutions for increasing μ is constructed. This results in branch *A* in Figures 6.1 and 6.2, showing the energy of

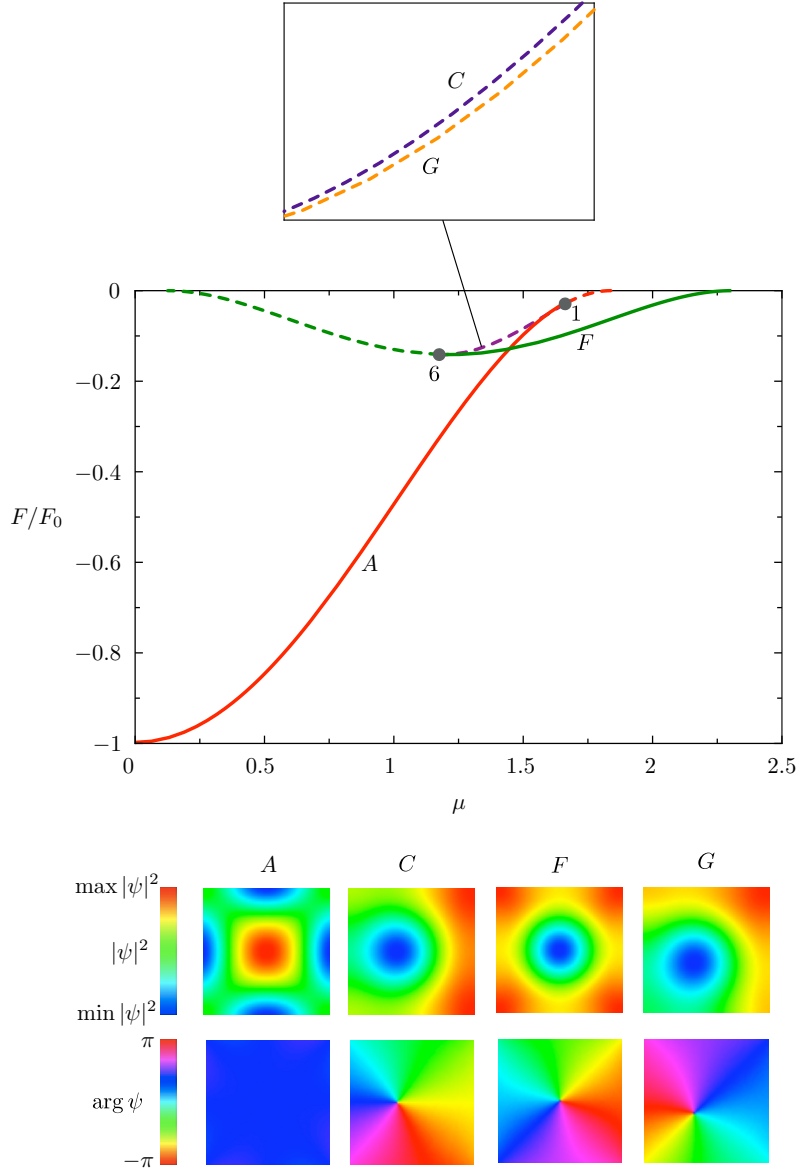


Fig. 6.1: Free energy of the solutions as a function of the strength of the applied magnetic field μ . Solid (dashed) lines represent stable (unstable) states. Branch A with D_4 symmetry starts at the homogeneous state with zero field and becomes unstable at bifurcation point 1. Branches G and C emerge from the bifurcation point, both characterized by a single vortex entering the domain; branch C has mirror symmetry along either the horizontal or the vertical center line, while branch G has mirror symmetry along one of the diagonals of the square domain. At bifurcation point 6, branches G and C connect to F , characterized by solutions with a single vortex in the center of the domain and full D_4 -symmetry.

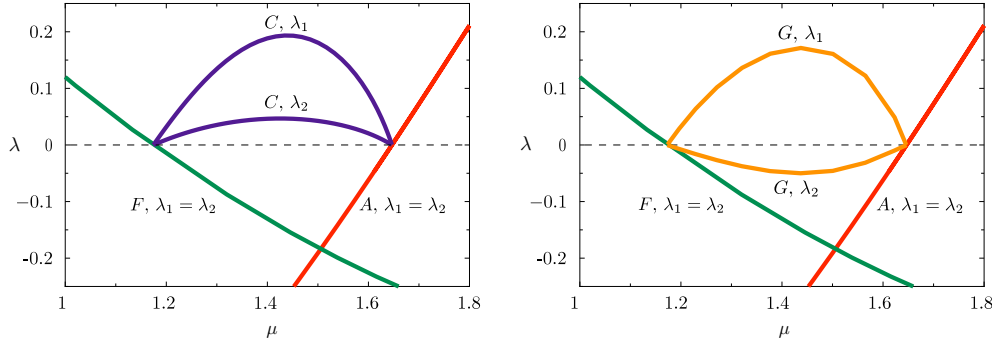


Fig. 6.2: The two largest eigenvalues of the Jacobian as a function of the applied magnetic field. We plot the eigenvalues close to bifurcation points 1 and 6, for each of the four solution branches in Figure 6.1. For field strength above $\mu = 1.646$ the main branch is unstable, while for fields strengths weaker than $\mu = 1.175$ the branch with a single vortex is unstable. We see that the largest eigenvalue of the main branch, which has multiplicity two, splits into two separate eigenvalues. Curve C has two unstable eigenmodes, while B has one stable and one unstable eigenmode. The colors reflect the branches in Figure 6.1.

the solution and the two most unstable eigenvalues of the Jacobian as a function of the field strength, respectively. For non-zero field strength, the solutions deviate from the homogeneous superconducting state, developing zones of low supercurrent density near the edges of the domain (see pattern A in Figure 6.1). As μ is increased, the states are characterized by a higher energy and they maintain full D_4 symmetry.

At field strength $\mu \approx 1.64$ (point 1 in Figure 6.1), an eigenvalue with multiplicity 2 becomes unstable. At this bifurcation point, one can apply the equivariant branching lemma: the Ginzburg–Landau equation is equivariant under the symmetries of the finite group D_4 and the eigenvalues cross the origin with non-zero speed, (see Figure 6.2). The lemma guarantees the existence of two solution branches emerging from the bifurcation, corresponding to the conjugacy classes of the isotropy subgroups $\langle \sigma \rangle$ and $\langle \sigma \rho \rangle$. They both have a one-dimensional fixed-point subspace. Hence, we expect two *different* families of solution branches, each containing four equivalent bifurcation curves with states belonging to one group orbit. The two families are found in the branches G and C of Figure 6.1.

Before describing curves G and C , the two curves that emerge from the bifurcation point, we continue to follow the original branch A for increasing μ . The state is now unstable and retains full D_4 symmetry. The magnetic field penetration increases from the boundaries until, at $\mu \approx 1.89$, the branch connects to the trivial state $\psi \equiv 0$, which corresponds to the normal state of the sample.

We now discuss the curves G and C , which have reduced symmetry and emerge from the bifurcation points 1 and 6. Curve C corresponds to solutions in which a single vortex moves in from one of the four sides of the square. These solutions belong to the conjugacy class of the subgroup $\langle \sigma \rangle$ and the single vortex sits either on the horizontally or vertically centered line.

The other family of solutions, on branch G , also features a single vortex entering the system, but along one of the diagonals. These solutions have an isotropy subgroup

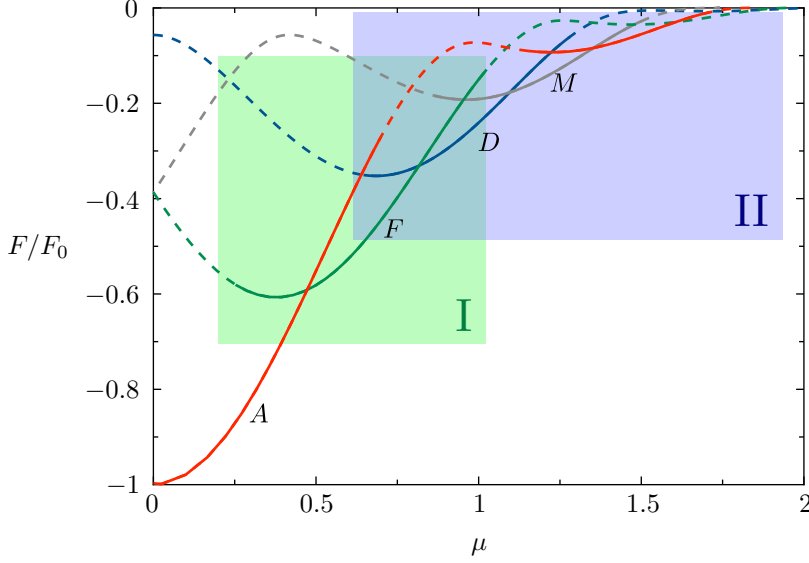


Fig. 6.3: The four main branches found for $d = 5.5$. The corresponding stable patterns with one vortex in the middle of the domain are presented in Figure 2.1. Solid (dashed) lines represent stable (unstable) states. Shaded areas are detailed in Figures 6.5 and 6.6.

that belongs to the conjugacy class of $\langle \sigma\rho \rangle$, hence their symmetry with respect to one of the diagonals.

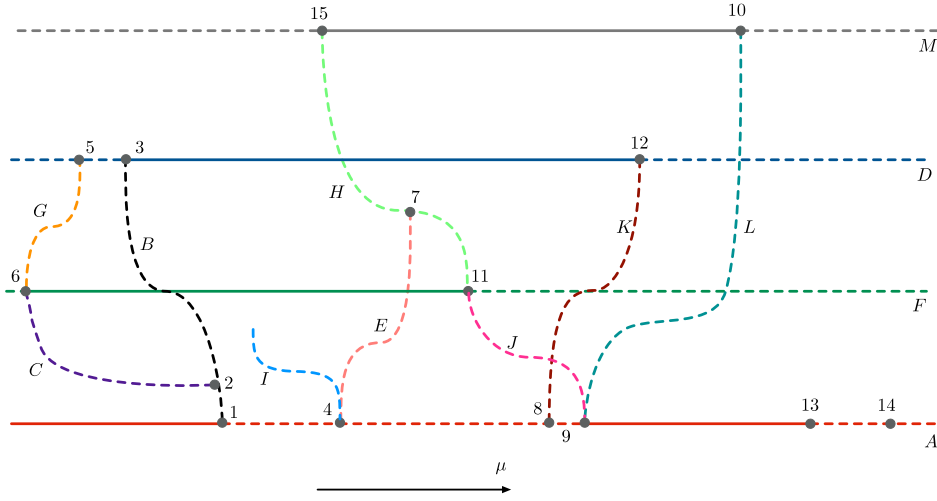
Solutions belonging to curves G and C are energetically similar, the latter having slightly higher energy, as it can be seen from the inset of Figure 6.1.

As we decrease the field strength from point 1 to point 6, the vortex moves along the center line for curve C , or along the diagonal for curve G , towards the center of the sample. At field strength $\mu \approx 1.18$ (point 6 in Figure 6.1), each solution features a vortex in the middle of the domain and enjoys full D_4 -symmetry. As we can see in Figures 6.1 and 6.2, bifurcation point 6 is analogous to bifurcation point 1, but it involves branch F instead of A .

The solution curve F in Figure 6.1 is characterized by a single vortex in the middle of the domain and is unstable for field strength weaker than $\mu \approx 1.18$. This solution branch extends all the way up to field strength $\mu \approx 2.30$ where it connects to the trivial zero solution.

In a physical experiment where the magnetic field is first increased and then decreased, we would expect to observe hysteresis: while increasing, the system would initially follow branch A , switching to F at point 1; conversely, for decreasing μ , we would pass from branch F to A , at point 6. Hysteresis effects such as this one have been discussed in [3], and observed experimentally in many superconducting systems (see also Figure 1.2).

6.2. Larger domain size ($d = 5.5$). In this section, we repeat the numerical experiment of Section 6.1 for a larger sample. In this context, it will be interesting to observe how the states of branch A destabilize: with edge length $d = 5.5$, more vortices can enter the domain, leading to a much more complicated bifurcation diagram.



Branch	Symmetry	$ \psi ^2$	$\arg \psi$	Branch	Symmetry	$ \psi ^2$	$\arg \psi$
A	$\langle \rho, \sigma \rangle$			H	$\langle \rho^2, \sigma \rangle$		
B	$\langle \rho^2, \sigma \rangle$			I	$\langle \sigma \rho \rangle$		
C	$\langle \sigma \rangle$			J	$\langle \sigma \rangle$		
D	$\langle \rho, \sigma \rangle$			K	$\langle \rho^2, \sigma \rangle$		
E	$\langle \sigma \rangle$			L	$\langle \sigma \rangle$		
F	$\langle \rho, \sigma \rangle$			M	$\langle \rho, \sigma \rangle$		
G	$\langle \sigma \rho \rangle$						

Fig. 6.4: Schematic of solution branches, bifurcations, and patterns found for $d = 5.5$.

Before starting to describe all the branches found by means of numerical continuation, we anticipate that we found four main branches, as opposed to the case $d = 3.0$, where we computed only two. The four main branches are collected in Figure 6.3: they are labeled F , D , M , A , corresponding to states with vorticities 1, 2, 3 and 4, respectively. Their stable segments, together with a few corresponding patterns, have

previously been sketched in Figure 2.1.

In the remainder of this section, we will concentrate on the two shaded areas (zone I and II) of Figure 6.3. In these regions, a series of symmetry-breaking bifurcations and cross-connecting branches are found.

As in the previous section, we start from the trivial homogeneous state $\psi \equiv 1$ at $\mu = 0$, and increase μ . The resulting solution branch, enjoying full D_4 symmetry, is labeled A and features four vortices entering the domain from the sides, similarly to what happens for $d = 3.0$. While this scenario resembles the one described in Section 6.1, the bifurcations occurring in zones I and II are quite different from the small-sized case, and we discuss them one by one in the remainder of this section. We refer the reader to the schematic in Figure 6.4, where we present all the branches, bifurcations, and representative patterns computed for $d = 5.5$.

6.2.1. Zone I. Branch A in zone I destabilizes with a *simple* eigenvalue, at field strength $\mu \approx 0.70$ (see point 1 in Figure 6.5). This mechanism is different from what we found the small-sized system, where an eigenvalue with multiplicity 2 becomes unstable. We can still apply the equivariant branching lemma: we expect a single family of solutions bifurcating from point 1, corresponding to a one-dimensional irreducible representation of D_4 [27].

The corresponding branch is labeled B in Figure 6.5. It belongs to the conjugacy class of the isotropy subgroup $\langle \rho^2, \sigma \rangle$, representing the mirror symmetries along horizontal and vertical center lines. When we follow this branch for decreasing values of μ , two vortices move simultaneously into the domain from opposite edges (left-right or top-bottom).

Along branch B , we find another symmetry-breaking bifurcation, point 2, where a second simple eigenvalue becomes unstable. This is shown in detail in the bottom panel of Figure 6.5, where we plot the negative value of the $L_2(\Omega_h)$ -norm in order to visualize the branches better. Branch C , emerging from point 2, has further reduced symmetry, corresponding to the conjugacy class $\langle \sigma \rangle$, that is, a family of branches with a single vortex on one of the center lines, away from the center.

On branch C , the vortex moves towards the middle of the sample and is connected via point 6, at $\mu \approx 0.25$, to branch F , the second main branch with full D_4 symmetry. A single vortex sits in the center of the domain throughout branch F and solutions on F are unstable for fields weaker than $\mu \approx 0.25$. This branch is similar to branch F in the small system described in the previous section.

Bifurcation point 6 features a null eigenvalue with multiplicity 2 and has the same symmetry properties as the bifurcation points discussed in Section 6.1. There, eigenvalues with multiplicity 2 became unstable on a branch with D_4 symmetry and two branches emerged with symmetries $\langle \sigma \rangle$ and $\langle \sigma\rho \rangle$ (see also Figure 6.1). In the current system, it has already been found that branch C with symmetry $\langle \sigma \rangle$ connects to point 6, and a second branch with symmetry $\langle \sigma\rho \rangle$ is to be expected. This branch has a single vortex on one of the diagonals and is shown as curve G in Figure 6.5. In contrast to the small size system, this curve does *not* connect to bifurcation point 1. Instead, it connects to curve D via bifurcation point 5.

A branch for which there is no equivalent in the smaller system is branch D in Figure 6.5, with a single vortex with multiplicity two (and hence phase change of $2 \times 2\pi$, a so-called *giant vortex*), in the middle of the domain. Branch D has full D_4 symmetry and is only stable for fields larger than $\mu \approx 0.64$. The corresponding bifurcation is marked by point 3 in Figure 6.5 and connects to branch B (see above).

At point 3, the two vortices of B merge into the giant vortex; similarly, branch G ,

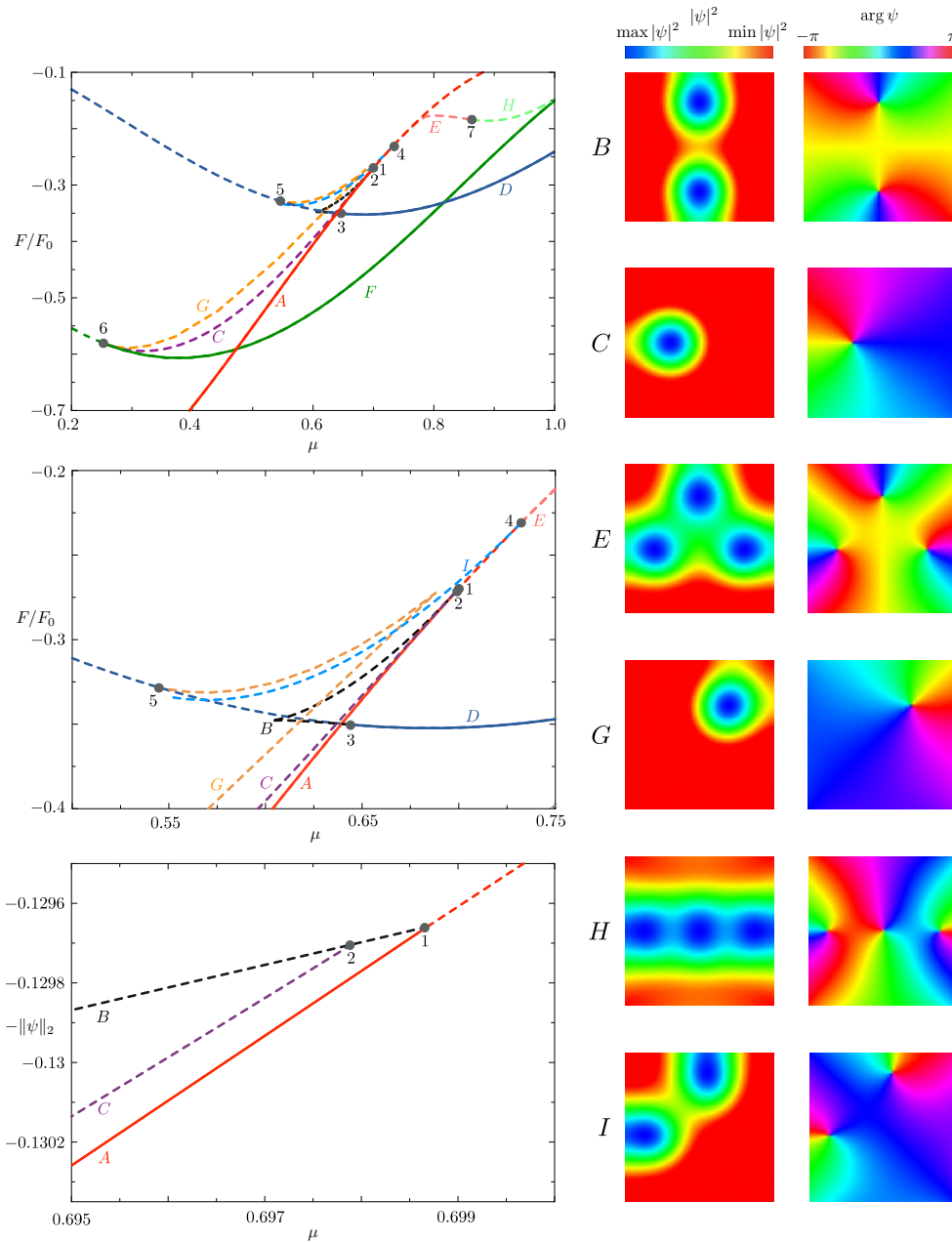


Fig. 6.5: Bifurcation diagrams and representative patterns found in zone I of Figure 6.3, in the case $d = 5.5$. Top and middle panels: free energy versus magnetic field intensity. Bottom panel: the negative norm of the solution is used in the bifurcation diagram, in order to separate points 1 and 2. Solid (dashed) lines represent stable (unstable) states.

which emerges from point 6 on branch F , connects to branch point 5 on branch D .

In the remaining part of zone I, we found that the main branch A has another instability, at bifurcation point 4. This bifurcation features a critical eigenvalue with multiplicity 2 and thus two families of solution branches emerge. Along branch E , three vortices enter the domain from three of the four sides of the domain. This branch corresponds to the conjugacy class of the subgroup $\langle\sigma\rangle$. The three vortices move towards the center of the system along the branch where they finally merge into a giant vortex with multiplicity 3 at point 7, connecting to branch H .

To conclude our exploration of zone I, we examined branch I , emerging from point 4 on the main branch A , for decreasing values of μ . Patterns on this branch have two vortices entering from two adjacent edges of the system. This branch is symmetric under reflections over one of the diagonals and corresponds to the conjugacy class of the subgroup $\langle\sigma\rho\rangle$.

6.2.2. Zone II. We now move to the upper part of the bifurcation diagram in Figure 6.1. An important difference from the small-sized system $d = 3$ is that the main branch A restabilizes as the field increases, as shown Figure 6.6.

As we increase μ along the main branch A , four vortices are moving in from the midpoints of the edges towards the center; the solutions maintain full D_4 symmetry. At field strength $\mu \approx 1.07$, the four vortices arrive at the center and form a giant vortex with multiplicity 4. As the field strengthens further, this giant vortex breaks up again and four separate vortices move away from the center along the *diagonals*. Note that there is no bifurcation point associated with this reorganization as none of the eigenvalues of the Jacobian crosses the origin.

At field strength $\mu \approx 1.14$, one of the unstable eigenvalues of bifurcation point 1 restabilizes. This yields bifurcation point 8 in Figure 6.6. From 8, branch K emerges and connects to branch D , with a vortex of multiplicity 2 in the center of the domain. Along branch K , two of the four vortices are pushed out of the sample along one of the center lines, while the two remaining reorganize into a giant vortex of multiplicity 2 (point 12). A sequence of patterns of branch K can be found in Figure 6.8.

Branch A restabilizes at field strength $\mu \approx 1.15$. The pattern with four symmetric vortices on the diagonals is now stable. The bifurcation point that marks this transition is labeled as point 9 in Figure 6.6. Two solution curves emerge from point 9, namely branches L and J .

Branch L , connecting to branch M via point 10, features five vortices, as can be seen in Figure 6.9: four vortices arranged symmetrically, rather close to the center, and a single antivortex at the center of the domain, so that the total vorticity of the configuration is 3. A giant vortex of multiplicity 3 is formed at bifurcation point 10 on branch M , where it is unstable. The fact that the vortices do not arrange as a giant vortex with vorticity 3 in a stable fashion has been predicted in [15]. Solutions on M are unstable for weak fields strengths (see bifurcation 15 in Figure 6.6).

In a similar way, branch J starts at point 9 and connects to point 11 on branch F for decreasing μ . The patterns along this branch are shown in the sequence of snapshots in Figure 6.7.

At field strength $\mu \approx 1.50$, the main branch A loses its stability again at point 13 in a scenario similar to the small-sized system discussed in Section 6.1. The eigenvalues of the Jacobian at this bifurcation point are degenerate and two branches emerge, each of which has a single vortex entering either along the diagonals or along the center lines. These branches connect to a stable branch with five vortices organized like the five dots on a dice. This branch has been omitted in the figures. Further on the main

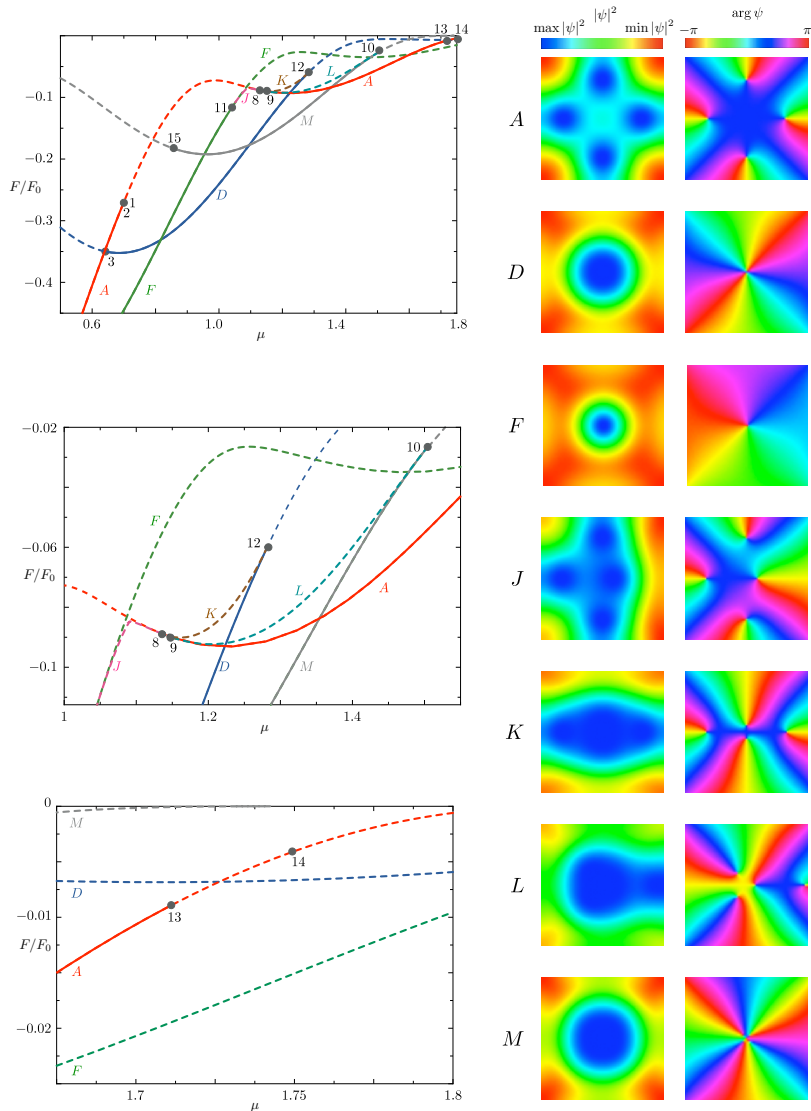


Fig. 6.6: Bifurcation diagrams and representative patterns found in zone II of Figure 6.3, in the case $d = 5.5$. Solid (dashed) lines represent stable (unstable) states.

branch, a second simple eigenvalue becomes unstable at point 14.

7. Discussion and conclusions. We have presented an initial exploration of the symmetry-breaking bifurcations of the vortex patterns as modeled by the Ginzburg–Landau equations. In the case of extreme type-II superconductors, we assumed a homogeneous applied magnetic field and showed how the vortices reorganize as the strength of the applied field is varied. In the small square domain ($d = 3$), we believe to have given a complete account of the instabilities of the system. For a larger system, the bifurcation diagram becomes much more complicated, and we found a large number of states and symmetry-breaking bifurcations.

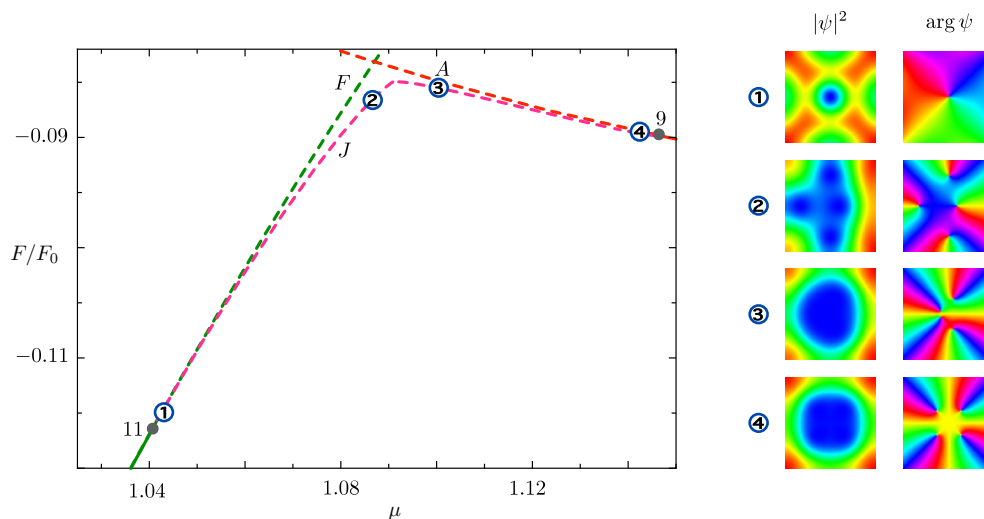


Fig. 6.7: Patterns of branch J in zone II (see Figure 6.6). Branch J bifurcates from branch F , which has a single vortex with multiplicity 1, and connects to branch A at bifurcation point 9.

The paper also presents a study of the symmetries of the system. It has been shown that the continuous system bears symmetries isomorphic to $S^1 \times D_4$. The discretization has been chosen in such a way that it preserves to machine accuracy both phase and geometric symmetries.

Owing to the symmetries of the system, it is possible to use the Equivariant Branching Lemma in order to predict the existence of new branches at symmetry-breaking bifurcations, and subsequently compute them numerically. To the best of the authors' knowledge, most of the patterns contained in this paper are unknown to the physics community: even though unstable patterns can not be obtained experimentally, we point out that the methodology proposed in this context could be effectively used to find new stable patterns.

The present paper analyzes the Ginzburg–Landau system on a square, but the same technique can be applied to all geometries with inherent symmetries, e.g., regular n -gons. It is not immediately obvious, though, how to choose the magnetic vector potential gauge such that the corresponding Ginzburg–Landau formulation remains equivariant with respect to D_n ; some work in this area has been done in [16]. Note that, for increasing n , the ever more complicated subgroup structure of D_n will lead to different bifurcation scenarios [23, 24].

In the present paper we simplified the Ginzburg–Landau equations considering the large- κ limit, where the equation for the magnetic vector potential \mathbf{A} decouples from the order parameter ψ . It will be necessary, in the future, to study the bifurcations in the coupled system for intermediate and small values of κ . However, this task will also pose new numerical challenges: the magnetic vector potential appears as an additional (vector-valued) unknown and its domain of definition is the whole space. In practice, the vector potential will approach its boundary condition defined by \mathbf{H}_0 sufficiently far away from the sample, but the validity of this approximation is still an open problem. The coupled system will in any case hold many more unknowns,

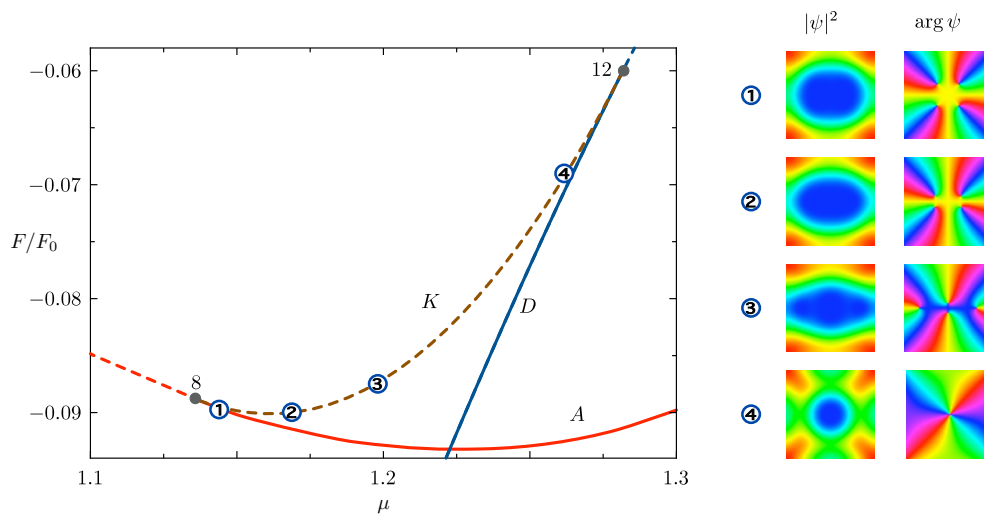


Fig. 6.8: Patterns on branch K in zone II (see Figure 6.6). The branch bifurcates off from branch A , with four vortices, at bifurcation point 8. Two of the four vortices are pushed out of the sample, while the remaining two reorganize into a giant vortex of multiplicity 2 at point 12.

and a robust preconditioning strategy for solving the appearing Jacobian systems will be crucial. However, the regularization technique that we employed for the extreme type-II case is applicable for finite values of κ and for generic spatial discretizations of the Ginzburg–Landau problem.

Nevertheless, we believe that results of this paper are a first step in understanding the bifurcations in the coupled Ginzburg–Landau system for various mesoscopic systems that are relevant for nanoscale devices. The approach proposed here opens up the possibility of a systematic exploration of the solution landscape in regions that are precluded to direct numerical simulation.

Acknowledgements. We acknowledge fruitful discussions with Golibjon Berdiyrov, Milorad Milošević, Ben Xu, Bart Partoens, Andrew G. Salinger, Eric T. Phipps, Mathieu Desroches, Rebecca Hoyle, and Philip Aston. We are also grateful to FWO-Vlaanderen for financial support through the project G017408N. Daniele Avitabile acknowledges EPSRC for funding his research with the grant EP/E032249/1.

Appendix A. Extension of Keller’s bordering lemma.

Keller’s bordering lemma [29] provides conditions on how a finite-dimensional linear system with a singularity of dimension 1 can be regularized by adding an additional unknown as well as an additional equation. In the present context, however, it is necessary to formulate the lemma in general vector spaces. Also, the defect of the present problem may be greater than one. Such situations occur, for example, in several branch points described in section 6. The following lemma shows that it is always possible to remove one of the singularities.

LEMMA A.1. *Let X, Y be \mathbb{K} -vector spaces and let $\mathcal{L} : X \rightarrow Y$ linear with $\dim \ker \mathcal{L} = k > 0$. Let further $b \in Y$, $d \in \mathbb{K}$, and $f : X \rightarrow \mathbb{K}$ a linear functional. Let*

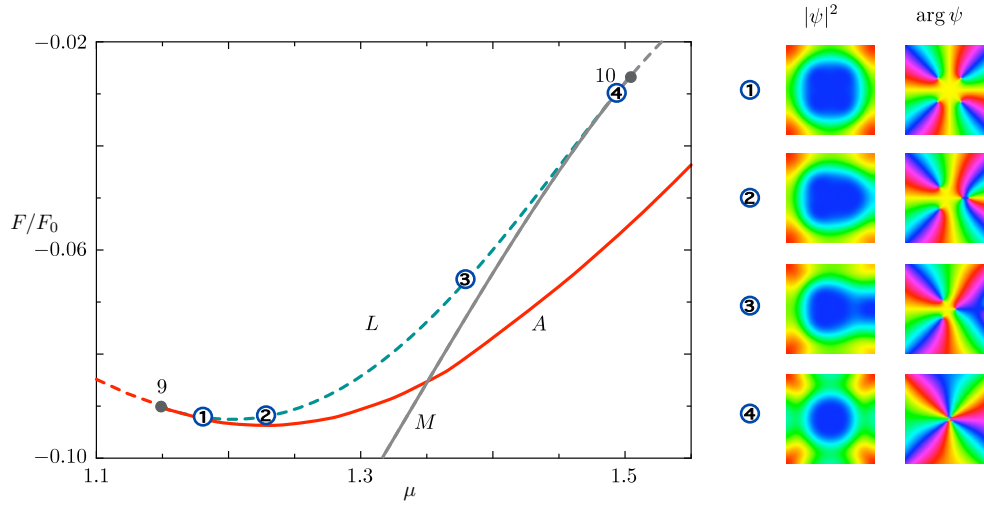


Fig. 6.9: Patterns on branch L in zone II (see Figure 6.6). The patterns show five vortices: four vortices are arranged symmetrically, rather close to the center, and a single antivortex sits at the very center of the domain, so that the total vorticity of the configuration is 3. At bifurcation point 10, when a giant vortex of multiplicity 3 is formed, the pattern becomes unstable, on branch M .

the operator $\tilde{\mathcal{L}} : X \times \mathbb{K} \rightarrow Y \times \mathbb{K}$ be defined by

$$\tilde{\mathcal{L}}\tilde{x} := \begin{pmatrix} \mathcal{L}x + b\xi \\ f(x) + d\xi \end{pmatrix}$$

for all $\tilde{x} = (x, \xi)^T \in X \times \mathbb{K}$. Then $\tilde{k} := \dim \ker \tilde{\mathcal{L}} < k$ if and only if $b \notin \mathcal{R}(\mathcal{L})$ and there exists a $v \in \ker \mathcal{L}$ with $f(v) \neq 0$.

Proof. On the one hand, let $b \notin \mathcal{R}(\mathcal{L})$ and let $v \in \ker \mathcal{L}$ with $f(v) \neq 0$. Let $\{(w^{(i)}, \xi_i)^T\}_{i=1}^{\tilde{k}} \subset X \times \mathbb{K}$ denote a basis of $\ker \tilde{\mathcal{L}}$, and take a $\tilde{x} \in \ker \tilde{\mathcal{L}}$,

$$\tilde{x} = \sum_{i=1}^{\tilde{k}} \alpha_i \begin{pmatrix} w^{(i)} \\ \xi_i \end{pmatrix}$$

with arbitrary $\alpha_i \in \mathbb{K}$. With this representation, we have

$$\begin{aligned} 0 &= \mathcal{L} \sum_{i=1}^{\tilde{k}} \alpha_i w^{(i)} + b \sum_{i=1}^{\tilde{k}} \alpha_i \xi_i, \\ 0 &= f \left(\sum_{i=1}^{\tilde{k}} \alpha_i w^{(i)} \right) + d \sum_{i=1}^{\tilde{k}} \alpha_i \xi_i. \end{aligned}$$

Because $b \notin \mathcal{R}(\mathcal{L})$, it must be $\sum_{i=1}^{\tilde{k}} \alpha_i \xi_i = 0$ as otherwise

$$b = \left(\sum_{i=1}^{\tilde{k}} \alpha_i \xi_i \right)^{-1} \sum_{i=1}^{\tilde{k}} \alpha_i \mathcal{L} w^{(i)} \in \mathcal{R}(\mathcal{L}).$$

Because the α_i are arbitrary, we have $\xi_i = 0$ for all i . Since $\{(w^{(i)}, \xi_i)^T\}_{i=1}^{\tilde{k}}$ is linearly independent in $X \times \mathbb{K}$ and all ξ_i are zero, $\{w^{(i)}\}_{i=1}^{\tilde{k}}$ is linearly independent in X . Besides that, it follows that $\sum_{i=1}^{\tilde{k}} \alpha_i w^{(i)} \in \ker \mathcal{L}$, and again because the α_i are arbitrary, we have $w^{(i)} \in \ker \mathcal{L}$ for all $i \in \{1, \dots, \tilde{k}\}$. Hence $\dim \ker \mathcal{L} \geq \tilde{k}$. One can exclude $\tilde{k} = \dim \ker \mathcal{L}$ since then $\ker \mathcal{L} = \text{span}\{w^{(i)}\}_{i=1}^{\tilde{k}}$, and at the same time $0 = f(\sum_{i=1}^{\tilde{k}} \alpha_i w^{(i)})$ for arbitrary α_i . This contradicts the assumption there is a $v \in \ker \mathcal{L}$ with $f(v) \neq 0$. Hence $\tilde{k} < k$.

On the other hand, let $\tilde{k} < k$. Consider the set $W := \ker \mathcal{L} \times \{0\}$. Obviously it is $\dim W = k$, and additionally for any $\tilde{w} = (w, 0)^T \in W$, one has

$$\tilde{L}\tilde{w} = \begin{pmatrix} \mathcal{L}(w) + 0 \cdot b \\ f(w) + 0 \cdot d \end{pmatrix} = \begin{pmatrix} 0 \\ f(w) \end{pmatrix}.$$

Hence, there must be a $v \in \ker \mathcal{L}$ with $f(v) \neq 0$ as otherwise $W \subseteq \ker \mathcal{L}$ and $\tilde{k} \geq k$.

It remains to be shown that $b \notin \mathcal{R}(\mathcal{L})$, and we will do this by contradiction: Suppose that $b \in \mathcal{R}(\mathcal{L})$ with a $p \in X$ such that $b = \mathcal{L}p$. Note that for any given $\alpha \in \mathbb{R}$, it is also $b = \mathcal{L}(p + \alpha v)$, where $v \in \ker \mathcal{L}$ such that $f(v) \neq 0$. Choose α such that $\alpha \neq (d - f(p))/f(v)$ and let $\hat{p} := p + \alpha v$ and $S := \{(w^{(i)} - \xi_i \hat{p}, \xi_i)^T\}_{i=1}^{\tilde{k}}$ with $\xi_i := f(w^{(i)})/(f(\hat{p}) - d)$. It can be checked that S is linearly independent by taking arbitrary $\{\beta_i\}_{i=1}^{\tilde{k}} \subset \mathbb{R}$ and demanding

$$0 \stackrel{!}{=} \sum_{i=1}^{\tilde{k}} \beta_i \begin{pmatrix} w^{(i)} - \xi_i \hat{p} \\ \xi_i \end{pmatrix}.$$

The second component yields $0 = \sum_{i=1}^{\tilde{k}} \beta_i \xi_i$, which results in

$$0 \stackrel{!}{=} \sum_{i=1}^{\tilde{k}} \beta_i \begin{pmatrix} w^{(i)} \\ 0 \end{pmatrix} + \sum_{i=1}^{\tilde{k}} \beta_i \xi_i \begin{pmatrix} -\hat{p} \\ 1 \end{pmatrix} = \sum_{i=1}^{\tilde{k}} \beta_i \begin{pmatrix} w^{(i)} \\ 0 \end{pmatrix}$$

The set $\{w^{(i)}\}_{i=1}^{\tilde{k}}$ is, however, linearly independent such that all β_i must vanish. Hence S is linearly independent. But S is also a subset of $\ker \tilde{\mathcal{L}}$ as

$$\tilde{\mathcal{L}} \begin{pmatrix} w^{(i)} - \xi_i \hat{p} \\ \xi_i \end{pmatrix} = \begin{pmatrix} \mathcal{L}(w^{(i)} - \xi_i \hat{p}) + b \xi_i \\ f(w^{(i)} - \xi_i \hat{p}) + d \xi_i \end{pmatrix} = \begin{pmatrix} \mathcal{L}w^{(i)} - \xi_i \mathcal{L}\hat{p} + b \xi_i \\ f(w^{(i)}) - \xi_i f(\hat{p}) + d \xi_i \end{pmatrix} = \begin{pmatrix} 0 \\ 0 \end{pmatrix}$$

This means that $\tilde{k} \geq k$, which is a contradiction.

□

REFERENCES

- [1] A.A. Abrikosov. Magnetic properties of superconductors of the second group. *Sov. Phys. JETP*, 5:1174, 1957.
- [2] A. Aftalion and S.J. Chapman. Asymptotic analysis of a secondary bifurcation of the one-dimensional Ginzburg-Landau equations of superconductivity. *SIAM Journal on Applied Mathematics*, 60(4):1157–1176, 2000.
- [3] A. Aftalion and Q. Du. The bifurcation diagrams for the Ginzburg-Landau system of superconductivity. *Physica D: Nonlinear Phenomena*, 163(1-2):94–105, 2002.
- [4] A. Aftalion and W.C. Tray. One the solutions of the the one-dimensional Ginzburg-Landau equations for superconductivity. *Physica D*, 132:214–232, 1999.
- [5] A.Y. Aladyshkin, A.V. Silhanek, W. Gillijns, and V.V. Moshchalkov. Nucleation of superconductivity and vortex matter in superconductor–ferromagnet hybrids. *Superconductor Science and Technology*, 22, 2009.

- [6] I.S. Aranson and L. Kramer. The world of the complex Ginzburg-Landau equation. *Reviews of Modern Physics*, 74(1):99–143, 2002.
- [7] J. Avron, I. Herbst, and B. Simon. Schrödinger operators with magnetic fields. I. General Interactions. *Duke Mathematical Journal*, 45(4):847–883, 1978.
- [8] C. Bacuta, J.H. Bramble, and J. Xu. Regularity estimates for elliptic boundary value problems with smooth data on polygonal domains. *Journal of Numerical Mathematics*, 11(2):75–94, June 2003.
- [9] B.J. Baelus and F.M. Peeters. Dependence of the vortex configuration on the geometry of mesoscopic flat samples. *Phys. Rev. B*, 65(10):104515, February 2002.
- [10] F. Bethuel, H. Brezis, and F. Hélein. *Ginzburg-Landau Vortices*. Springer, 1994.
- [11] W.J. Beyn and V. Thümmmler. Freezing solutions of equivariant evolution equations. *SIAM Journal on Applied Dynamical Systems*, 3(2):85–116, 2004.
- [12] W.J. Beyn and V. Thümmmler. *Numerical Continuation Methods for Dynamical Systems*, chapter Phase conditions, symmetries and PDE continuation, pages 301–330. Canopus, Springer, 2007.
- [13] L.R.E. Cabral, B.J. Baelus, and F.M. Peeters. From vortex molecules to the Abrikosov lattice in thin mesoscopic superconducting disks. *Phys. Rev. B*, 70(14), October 2004.
- [14] A.R. Champneys and B. Sandstede. *Numerical Continuation Methods for Dynamical Systems*, chapter Numerical computation of coherent structures, pages 331–358. Canopus, Springer, 2007.
- [15] L.F. Chibotaru, A. Ceulemans, V. Bruyndoncx, and V.V. Moshchalkov. Symmetry-induced formation of antivortices in mesoscopic superconductors. *Nature*, 42(4):555–598, 2000.
- [16] L.F. Chibotaru, A. Ceulemans, M. Morelle, G. Teniers, C. Carballeira, and V.V. Moshchalkov. Ginzburg–Landau description of confinement and quantization effects in mesoscopic superconductors. *Journal of Mathematical Physics*, 46(9), September 2005.
- [17] E.N. Dancer and S.P. Hastings. On the global bifurcation diagram for the one-dimensional Ginzburg–Landau model of superconductivity. *European Journal of Applied Mathematics*, 11(03):271–291, 2000.
- [18] J.W. Demmel. *Applied numerical linear algebra*. Society for Industrial and Applied Mathematics, 1997.
- [19] P. Singha Deo, V.A. Schweigert, F.M. Peeters, and A.K. Geim. Magnetization of mesoscopic superconducting disks. *Phys. Rev. Lett.*, 79(23):4653–4656, December 1997.
- [20] Q. Du. Discrete gauge invariant approximations of a time dependent Ginzburg–Landau model of superconductivity. *Math. Comput.*, 67(223):965–986, 1998.
- [21] Q. Du, M.D. Gunzburger, and J.S. Peterson. Analysis and approximation of the Ginzburg–Landau model of superconductivity. *SIAM Rev.*, 34:54–81, March 1992.
- [22] Q. Du and L. Ju. Numerical simulations of the quantized vortices on a thin superconducting hollow sphere. *Journal of Computational Physics*, 201:511–530, 2004.
- [23] M. Golubitsky, D.G. Schaeffer, and I. Stewart. *Singularities and groups in bifurcation theory*. Springer Verlag, 1988.
- [24] M. Golubitsky and I. Stewart. *The symmetry perspective*. Birkhäuser, 2002.
- [25] B.B. Goodman. Type ii superconductors. *Reports on progress in physics*, 29:445, 1966.
- [26] M.A. Heroux and J.M. Willenbring. Trilinos Users Guide. Technical Report SAND2003-2952, Sandia National Laboratories, 2003.
- [27] R. Hoyle. *Pattern formation*. Cambridge University Press, 2006.
- [28] H.G. Kaper and M.K. Kwong. Vortex configurations in type-II superconducting films. *Journal of Computational Physics*, 119(1):120–131, June 1995.
- [29] H.B. Keller. Numerical solution of bifurcation and nonlinear eigenvalue problems. In Paul H. Rabinowitz, editor, *Applications of bifurcation theory: proceedings of an advanced seminar*, pages 359–384, University of Wisconsin–Madison, October 1976. Academic Press, New York.
- [30] C.T. Kelley. *Iterative Methods for Linear and Nonlinear Equations*, volume 16 of *Frontiers in Applied Mathematics*. SIAM, 1995.
- [31] B. Krauskopf. *Numerical Continuation Methods for Dynamical Systems: Path following and boundary value problems*. Springer Verlag, 2007.
- [32] F.-H. Lin and Q. Du. Ginzburg–Landau vortices: dynamics, pinning, and hysteresis. *SIAM J. Math. Anal.*, 28(6):1265–1293, 1997.
- [33] C.W. Rowley, I.G. Kevrekidis, J.E. Marsden, and K. Lust. Reduction and reconstruction for self-similar dynamical systems. *Nonlinearity*, 16:1257, 2003.
- [34] E. Sandier and S. Serfaty. *Vortices in the magnetic Ginzburg-Landau model*. Birkhäuser, 2007.
- [35] V.A. Schweigert, F.M. Peeters, and P. Singha Deo. Vortex phase diagram for mesoscopic superconducting disks. *Phys. Rev. Lett.*, 81(13):2783–2786, September 1998.

- [36] D.G. Schweitzer and M. Garber. Hysteresis in superconductors. II. Experimental tests for critical states. *Phys. Rev.*, 160(2):348–358, August 1967.